Published in final edited form as:
J Mol Biol. 2013 July 24; 425(14): 2509–2528. doi:10.1016/j.jmb.2013.04.001.

Ligand induced dynamics changes in extended PDZ domains from NHERF1

Shibani Bhattacharya[1,*], **Jeong Ho Ju**[3,*], **Natalia Orlova**[3], **Jahan Ali Khajeh**[3], **David Cowburn**[2], and **Zimei Bu**[3]

[1] New York Structural Biology Center, 89 Convent Avenue, New York, NY, 10027, USA.

[2]Depts of Biochemistry, and of Physiology and Biophysics, Albert Einstein College of Medicine of Yeshiva University, Bronx, NY, 10461.

[3] Department of Chemistry, City College of New York, New York, New York, USA, 10031.

Abstract

The multi-domain scaffolding protein NHERF1 modulates the assembly and intracellular trafficking of various transmembrane receptors and ion-transport proteins. The two PDZ domains of NHERF1 possess very different ligand-binding capabilities: PDZ1 recognizes a variety of membrane proteins with high affinity, while PDZ2 only binds limited number of target proteins. Here using NMR, we have determined the structural and dynamic mechanisms that differentiate the binding affinities of the two PDZ domains, for the Type 1 PDZ-binding motif (QD**T**R**L**) in the carboxyl-terminus of CFTR. Similar to PDZ2, we have identified a helix-turn-helix subdomain coupled to the canonical PDZ1 domain. The *extended* PDZ1 domain is highly flexible with correlated backbone motions on fast and slow timescales, while the *extended* PDZ2 domain is relatively rigid. The malleability of the extended PDZ1 structure facilitates the transmission of conformational changes at the ligand-binding site to the remote helix-turn-helix extension. By contrast, ligand-binding has only modest effects on the conformation and dynamics of the extended PDZ2 domain. The study shows that ligand induced structural and dynamic changes coupled with sequence variation at the putative PDZ binding site dictate ligand selectivity and binding affinity of the two PDZ domains of NHERF1.

Introduction

In eukaryotic cell signaling, the PDZ domains constitute one of the most important classes of cytoplasmic adaptor proteins that function as structural components of modular scaffolds involved in mediating protein-protein interactions [1; 2]. A prototypical PDZ domain possess a αβ globular fold that binds specifically to linear carboxyl terminal peptides [3] and in rare cases to internal β hairpin forming motifs [4] and lipids [5]. The linkage of multiple PDZ

*Authors have contributed equally to the work

domains with varying target specificities appears to be a familiar evolutionary strategy to expand the vast repertoire of biological binding partners in macromolecular assemblies [1]. The mammalian NHERF family of proteins with two or more homologous PDZ domains represents the functional synergy of similar scaffolds linked by a common chain in regulating downstream signaling [6; 7; 8; 9].

NHERF1, also called ezrin binding protein or EBP50 [10], consists of two PDZ domains and a carboxy-terminal ezrin binding domain (EBD) juxtaposed with a PDZ motif (-F**S**N**L**^{358}) (**Figure 1A**). Association of Ezrin releases the autoinhibited conformation from intra-molecular head-to-tail interactions between PDZ2 and the carboxy-terminal PDZ binding motif in EBD [11; 12; 13; 14; 15; 16]. The bivalent NHERF1 is active predominantly in trafficking and function of a number of membrane proteins, including ion channels [7] and GPCR coupled receptors [17; 18; 19] facilitated through association with ezrin and other ERM (ezrin-radixin-moesin) proteins from the actin cytoskeleton [20].

A notable target of NHERF1 is the cystic fibrosis transmembrane conductance regulator (CFTR) [21; 22], a chloride ion channel that regulates the flow of fluid transport across the apical membrane of epithelial cells. Mutations or deletions in the *CFTR* gene have fatal consequences on the stability and gating of the transmembrane ion channel, a leading cause of cystic fibrosis [23]. The Type 1 carboxy-terminal PDZ binding motif of CFTR (-D**T**R**L**) mediates a crucial interaction with NHERF1, a component of the CFTR interactome [24]. NHERF1 has been demonstrated to stimulate CFTR activity by multimerization [25], regulate endocytic recycling [26] and form heterologous complexes with β2 adrenergic receptors [27]. Overexpression of NHERF1 in human airway cells accompanied by increased cytoskeleton organization has been demonstrated to rescue the most common genetic mutation ΔF508 CFTR targeted for degradation in the pathogenesis of cystic fibrosis [28].

Despite high sequence identity (58%), the PDZ1 domain from NHERF1 targets a disproportionately large number of cellular binding partners (>50) compared to a far more selective PDZ2 domain [29]. So far the binding site sequence variation or static view of the X-ray structures has failed to provide an adequate rationale for the extraordinary ability of the PDZ1 domain to recognize diverse targets [30; 31; 32]. Traditionally the high propensity for mutations in the active site of the PDZ domains has been cited as the primary source of ligand specificity [33; 34]. However the generic target affinity and biological function of the canonical PDZ domain can be altered dramatically by multiple factors, including conformational dynamics of the isolated [35; 36] or coupled domains [18; 37] and unique structural modifications [38; 39; 40; 41; 42].

Previously we have identified a novel helix-loop-helix extension in the PDZ2 domain from NHERF1 that plays a critical role in transforming an unstable PDZ fold to a functional scaffold with enhanced affinity for selected target peptides [14]. The twenty residue extension rich in hydrophobic residues is highly conserved across various species of NHERF1 and hence very likely to adopt a similar structural role in each example (**Figure 1C**). Interestingly, the alignment of the N-terminal PDZ1 domains revealed greater variation in the carboxy-terminal sequence across species (**Figure 1B**). Based on the sequence identity

along α3, we hypothesize that the PDZ1 domain is likely extended by similar helical structure but the presence of α4 helix was not conclusive.

To confirm our hypothesis, in this study we have determined the boundaries of the PDZ1 domain of NHERF1 by NMR spectroscopy, and compared the ligand dependent structural and dynamic changes in the *extended* PDZ1 and PDZ2 domains. Previous studies have collectively demonstrated that the carboxy-terminal Type 1 motif (-QD**T**R**L**) of CFTR has a significantly higher binding affinity for PDZ1 than the PDZ2 domain [11; 25; 43]. To address the role of sequence variations in dictating the selectivity of the binding site, we have determined the solution structures of the *extended* PDZ1 and PDZ2 domains of NHERF1 in complex with a consensus binding motif from CFTR consisting of five residues (QD**T**R**L**) by NMR. Furthermore, the long-range impact of ligand induced allostery mediated by the plasticity of the *extended* PDZ1 and PDZ2 structures were evaluated by measuring the changes in amide nitrogen relaxation rates along the backbone. Our results reveal *unique* intermolecular contacts at the ligand-binding site in concert with correlated motions on multiple time scales in the extended PDZ structures, determined the relative promiscuity and affinity of PDZ ligand binding.

RESULTS

Overview of the extended apo PDZ1 domain structure

Our previous structural study of the PDZ2 domain and the contiguous carboxy-terminal region (**PDZ2CT**) by NMR spectroscopy revealed the presence of a novel α-helix-loop-(3_{10}) helix motif (**HLG**) coupled to the putative PDZ2 domain (residues 154-231) [14]. The conventional PDZ2 (residues 153-231) domain is marginally stable with much lower affinity for ligands than the *extended* $PDZ2^{270}$ (residues 153-270) structure (**Table 1**). The similarities in the carboxy-terminal sequence between the PDZ domains suggest the presence of some helical structure extending beyond the putative PDZ1 domain (**Figure 1**).

Herein we describe the NMR structure of the extended $PDZ1^{120}$ domain in solution, which includes the prototype PDZ fold (residues 1-91) composed of a six stranded β-sheet linked by helices α1 and α2 (**Figure 2A and 2B**). The ligand-binding cleft is enclosed between the hydrophobic residues from β2, α2 and the highly conserved glycine rich (–GYGF-) carboxylate binding (**CBD**) β1-β2 loop (**Figure 2B**). Similar to $PDZ2^{270}$, the carboxy-terminal thirty residues in $PDZ1^{120}$ forms a HLG subdomain, consisting of α-helix (α3), extended loop and 3_{10}-helix (α4) (**Figure 2C**). The long range contacts between the domains are mediated by hydrophobic side-chain interactions involving β1 (Leu14), β6 (Leu89 and Val91) and α4 (Val106, Leu110 and Leu111) (**Figure 2D**). The hydrophobic core is stabilized by additional interactions between the α3–α4 helices and several residues (Phe8-Thr9-Pro12) from the unstructured N-terminus.

Favorable long-range electrostatic interactions between charged residues impart further stability to the HLG extension (**Figure 3**). In the $PDZ1^{120}$ structure, intra-helical *i*,*i*+4 charged side-chain pairs stabilize α3 and potentiate long range contacts between Glu61 from β4 strand and Arg107 from the loop connecting α3 and α4 helices (**Figure 3A**). The single Glu61->Gly61 mutation results in significant chemical shift perturbation in the entire HLG

subdomain, including N-terminal residues, β4-β5 strands and α3-α4 helices (**Figure 3C**) without any loss of secondary structure in the helices (**Supplementary Figure 1**). It is very likely that the loss of the Glu61-Arg107 interaction increases the flexibility of the extended loop connecting α3-α4 which in turn triggers some rearrangement within the HLG subdomain.

Within usual limits [44], the length of the canonical PDZ1^{120} domain (residues 13-91) superimposes with that of PDZ2^{270} (residues (153-231) structural ensemble quite well with a backbone RMSD of 0.95 Å but is significantly worse, with RMSD of 1.5 Å when the HLG extensions are included in the backbone alignment (**Figure 2C**). Despite the apparent similarities in the secondary structure, the inter-helical packing in the HLG subdomain of the *extended* PDZ1 and that of PDZ2 domains are quite different because of sequence variation (**Figure 1B & 1C)**. The notable substitutions include the two aromatic side-chains in PDZ2^{270}, Phe238 and Phe239, replaced by Gln98 and Leu99 in PDZ1^{120}, respectively, resulting in loss of hydrophobic packing (**Figure 2D & 2E**). Likewise the putative salt bridge between Glu61 in PDZ1^{120} and Arg107 from the α3-α4 loop is modified by corresponding mutation to Ser247 in PDZ2^{270}. In a significant fraction of NMR structures (>85%), the side-chain of Glu201 can reorient itself to form a hydrogen bond with Gln248^{N} while Ser247 is paired with His250 (His250$^{H\delta1}$ – Ser247^{N} and His250^{H} – Ser247^{O}) to stabilize α4 helix (**Figure 3B and Supplementary Figure 2B**).

The combined effect of the various natural mutations on the conformation of the HLG extension from the PDZ1^{120} domain is to make it more floppy compared to PDZ2^{270}. The dynamics are reflected by the unfavorable exchange broadening of multiple amide resonances (Val106-Leu110) in the extended loop connecting the HLG helices.

In summary, the extended PDZ domains of NHERF1 share a stable binding scaffold attached to a variable structural module tethered by long-range hydrophobic and electrostatic interactions. The relative contribution of the variable motif to the overall stability of the extended PDZ structures was evaluated from the mid-point of thermal unfolding (Tm) reported in **Table 1**. The putative PDZ2 scaffold does not exist as an independent viable structure and in this instance the significantly enhanced stability of the extended domain is crucial and translated directly into much higher affinities for target peptides [14]. Based on the small increase in Tm values, the dynamic HLG subdomain from PDZ1^{120} appears to be much less critical for the overall stability of the binding scaffold. While it has a modest impact on the increased binding affinity for CFTR-C, the identification of specific disease related mutations (L110V) in defective Parathyroid Hormone Type 1 Receptor (PTH1R) function suggests the extended PDZ1 structure is essential for association with other targets [19; 45]. Based on our structure we hypothesize the smaller hydrophobic side-chain is very likely to disrupt the marginally stable HLG subdomain and hence reduce affinity for the PDZ binding motif from PTH1R [19]. An open question is the extent to which any loss of structure in the HLG subdomain increases the configurational flexibility of the linker between the tandem PDZ domains and thus inhibits the assembly of a larger complex of PTH1R and ezrin mediated by NHERF1. Structural characterization of the intact NHERF1 with its various targets is necessary to address these questions.

Structural basis for Type 1 PDZ-binding motif recognition

The pentapeptide QD**T**R**L** in CFTR-C is a classic Type 1 PDZ-binding motif. The CFTR-C peptide binds to PDZ1^{120} (K_d ~ 365 nM) with nearly three-fold higher affinity compared to PDZ2^{270} (K_d ~ 1079 nM) (**Table 1**). Despite the large difference in binding affinities, the chemical shift perturbation of the amide resonances suggests similar binding sites for the peptide (**Supplementary Figure 2**). To understand how the binding site sequence variation alters specific intermolecular contacts, we have determined the high resolution NMR structures of the complexes of CFTR-C peptide bound to PDZ1^{120} and PDZ2^{270}, respectively, using standard NMR based methods (**Figure 4**). A summary of the statistics is presented in **Table 2**.

The high backbone RMSD (~1.9 Å) of the structural superposition of apo and peptide bound PDZ1^{120} revealed rearrangement in the hydrophobic core of the canonical domain coupled to long-range conformational changes triggered in the HLG subdomain (**Figure 4C**). The major difference between the structures is in the movement of the α2 helix by ~10° to close the width of the binding cleft with the β2 strand. The conformational changes in the β-sandwich structure are clearly propagated by the inter-domain contacts to the remote structure. In contrast the binding scaffold from the PDZ2^{270} domain is superimposable (~1.0 Å) in the presence and absence of ligand with nominal realignment of the helices in the remote structure (**Figure 4F**).

In both PDZ1^{120} and PDZ2^{270} complexes, the residues that are involved directly in binding the peptide are highlighted in **Figure 5A**. The CFTR-C peptide is aligned within the putative PDZ binding site in an extended configuration anchored by residues from β2 strand and α2 helix (**Figures 5B-5E**). In this particular configuration, the backbone of the C-terminal residues are highly ordered by the formation of pairwise hydrogen bonds between the peptide and the backbone atoms of carboxylate binding loop and β2 strand (**Figure 5C and 5E**), supported by the observation of intermolecular H^N-H^N and H^N-H^α NOEs. The heavy atom distances between potential hydrogen bond donor-acceptor pairs from NMR structure are summarized in **Table 3**, along with those from the previously published X-ray structure of the canonical PDZ1 domain complexed with an identical CFTR-C peptide [30; 46]. There is strong agreement between the NMR and the X-ray structures on the critical H-bond interactions and the backbone heavy atoms (residues 13-91) are superimposable with RMSD of 1.3 Å.

In the PDZ2^{270} complex structure, similar to PDZ1^{120} the ligand is secured primarily by a network of hydrogen bonds between the carboxy-terminal oxygen atoms of Leu^0 from the CFTR-C peptide and the exposed backbone atoms of Tyr164 and Gly165 in the conserved β1-β2 loop (-GYGF-) from the PDZ fold (**Figure 5E**). The methyl groups of Leu^0 sterically fit into a hydrophobic cavity encircled by the aromatic side-chains of Tyr164, Phe166 (β2) and Ile219 (α2) in the binding cleft. The extended backbone of the peptide is reinforced by additional H-bond pairs involving the β2-strand, Leu^0 N-Phe166 O and Thr^{-2} O -Leu168 N respectively. The peptide aligned along the length of the α2 helix makes multiple hydrophobic contacts with Val216 and Ile219 that are strengthened further by H-bond between Thr^{-2} Oγ1 and His212 Hε2 atoms (**Table 3**). Thus, the mode of recognition of

crucial residues Leu^{0} and Thr^{-2}, in the Type 1 motif are conserved in the two PDZ domains of NHERF1. Indeed, mutating either residue in CFTR has a debilitating effect on its ability to associate with NHERF1 [21; 47].

Tuning PDZ domain peptide binding affinities by electrostatic interactions

The sequence variation within the binding site implies that PDZ1 and PDZ2 from NHERF1 will encode different binding affinities for various Type 1 motifs (**Figure 5A**). While the generic peptide affinity is derived from hydrogen bonds formed between the carboxy-terminal hydrophobic residue from the Type 1 motif with the carboxylate binding loop from the PDZ domains, the affinity is evidently fine-tuned by variable interactions [33]. Of particular interest is the role of the charged residues Arg^{-1} and Asp^{-3} from the Type 1 motif of the CFTR-C peptide and the nature of their interactions with the protein.

The electrostatic surface map of PDZ1 domain shows excellent complementarity exists between the charged side-chains of the peptide and protein at the complex interface (**Figure 6A**). In the $PDZ1^{120}$ complex, the bidendate guanido group of Arg^{-1} is strategically located with respect to its ability to form H-bond with the Glu43 COO^{-} group. Likewise, the Asp^{-3} COO^{-} group is favorably positioned to interact with both the imidazole group of His27 (**Figure 5C**) and Arg40 side-chain (**Figure 6A**). Key natural mutations in the $PDZ2^{270}$ binding site eliminate the favorable electrostatic interactions between the peptide and PDZ1 domain. The Glu43->Asp183 substitution in the PDZ2 α1 helix is detrimental to the formation of a typical H-bond with the penultimate Arg^{-1} by increasing the average distance between the heavy atoms consistent with molecular dynamics simulations [48]. Based on the donor-acceptor distances, the His27->Asn167 substitution in PDZ2 very likely favors H-bond formation between the Asn167 ND_2 group and the peptide backbone instead of the Asp^{-3} COO^{-} group (**Table 3**). In this case Asp^{-3} COO^{-} group can rearrange to interact with either His169 (**Figure 5E**) or Arg180 side-chains (**Figure 6D**).

In order to rationalize the nearly threefold higher binding affinity of the CFTR-C peptide for $PDZ1^{120}$ compared to the $PDZ2^{270}$ domain, we have measured the impact of the two mutations, His27->Asn27 and Glu43->Asp43 on the affinity (**Table 1**). The dramatic loss of ligand affinity imposed by the single mutation Glu43->Asp43 in $PDZ1^{120}$ conclusively proves the importance of preserving the H-bond with the positively charged Arg^{-1} side-chain from the CFTR-C peptide. In contrast, the His27->Asn27 mutation shows a modest decrease in binding affinity, reflecting the elimination of a relatively weak salt bridge. The low target affinity of the double mutant confirms that Glu43 in PDZ1 is crucial for high binding affinity of Type 1 motif, with a positive charge at the penultimate (P^{-1}) position from all peptide sequences.

Interestingly, the impaired association between the intact CFTR-C domain and the double mutant of $PDZ1^{120}$ (~1100 nM) is recovered dramatically in the $PDZ2^{270}$ domain (~267 nM), despite sharing identical binding site contacts involving β2 strand, α1 and α2 helix (**Figure 5A**). Furthermore, the CFTR-C domain binds to the PDZ domains in a length dependent manner [43] and this trend is most notable for the $PDZ2^{270}$ domain whose affinity for the peptide is drastically reduced by a factor of three (**Table 1**). To map the site for potential upstream interactions that could augment the overall affinity, we compared the

chemical shift perturbation between the extended PDZ domains in complex with the pentapeptide and the longer 70 residue CFTR-C domain. The survey of the backbone chemical shift perturbation revealed the putative binding sites of the peptide and the longer CFTR-C domain overlap with the most significant differences located in the β2-β3 loop region of the complex (**Figure 6C and 6F**). The upstream sequence from the longer CFTR carboxy-terminal tail has an unusual repeat of acidic residues (-K**EE**T**EE**VQD**T**R**L**). As revealed by the electrostatic surface map of the PDZ2^{270} domain (**Figure 6D)**, the positively charged cluster from the β2-β3 loop (K172, K174) and surrounding residues (R198, Q196 and Q211) collectively present a favorable binding patch for the negative charge. The overall binding affinity is enhanced by the contribution from favorable electrostatic interactions compensating for any loss of the Glu43 and Arg^{-1} salt bridge within the PDZ2^{270} binding pocket. The weakening of these secondary interactions involving the upstream sequence in the PDZ1^{120} domain offers a plausible explanation for the modest length dependence of affinity (**Table 1**).

Therefore, both PDZ1^{120} and PDZ2^{270} of NHERF1 recognize the Type 1 motif from the CFTR-C peptide but the affinities are modulated by distinct structural features. The PDZ1^{120} binding scaffold is malleable and the sequence along α1-α2 and β2-β3 optimized for recognizing the carboxy-terminal four residues (-D**T**R**L**) from CFTR-C resulting in high affinity. In contrast PDZ2^{270} captures the primary anchors Leu^{0} and Thr^{-2} from the Type 1 motif without any conformational change. The binding site sequence is not optimized for either Arg^{-1} or Asp^{-3} leading to reduced peptide affinity. Nevertheless, the loss of affinity is recovered by favorable electrostatic interactions between the β2-β3 loop in PDZ2, and the negatively charged upstream sequence from the intact CFTR-C domain. Thus, the ability of either PDZ1 or PDZ2 domain to form favorable electrostatic interactions with the target peptide is important for selectivity, and plays a pivotal role in fine-tuning the binding affinity. The charge distribution at the binding surface is also crucial for *electrostatic steering* of ligands to the appropriate PDZ domain.

Sequence dependent ligand-binding specificities of PDZ domains

The NHERF1 PDZ1 domain is highly promiscuous and capable of binding to a broad array of peptide sequences, while PDZ2 recognizes fewer ligands [48; 49]. One approach to rationalize this observation is to employ the vast network of known PDZ interactions to identify the amino acid propensities in the target sequence for each domain. A quantitative measure of the amino acid probabilities is represented by the position weight matrix calculated for each binding pocket associated with a particular position along the sequence [34] (**Figure 5G**). The veracity of the analysis was confirmed by the strong preference for Leu^{0} and Thr^{-2} at the invariant positions of the typical Type 1 PDZ motif. The high probability of these side-chains is in agreement with the conserved intermolecular contacts observed within the real CFTR-C peptide-protein complex structures. The most glaring difference between the domains is dictated by the remarkable lack of specificity for any single type of side-chain in the P^{-1} binding pocket of the PDZ1 domain which as noted earlier, plays a critical role in improving the overall binding affinity. The ability to accommodate diverse residue types can be reasoned from the versatile binding pocket enclosed by a cluster of hydrophobic side-chains (Phe26, His27, Leu41) and the fortuitous

proximity of H-bonding partners (His27, Glu43). In the PDZ2 domain, the predominantly polar character of the P^{-1} pocket (Phe166, Asn167, Ser181 and Asp183) is detrimental for typical hydrophobic side-chains. Instead it has unusual affinity for the amphiphilic side-chain of Tryptophan entirely consistent with experimental scanning of peptide libraries [22]. Owing to sequence variation around the P^{-3} binding pocket, this particular position in the target shows little specificity.

Thus, the *hydrophobicity* of the P^{-1} pocket is one of the contributing factors in the broad specificity of the $PDZ1^{120}$ domain and when combined with favorable electrostatic pairing of side-chains from the target offers a powerful strategy to attract various ligands with high affinity.

The extended PDZ1 structure is more dynamic than PDZ2

In order to assess the effects of protein plasticity on ligand recognition and binding affinity, we have measured the field-dependent amide nitrogen relaxation rates of the extended PDZ1 and PDZ2 domains in the presence and absence of ligands. The relaxation data were analyzed using reduced spectral density mapping approach [50; 51]. Attempts to extract a single rotational correlation time or diffusion tensor needed for Modelfree analysis [52] was not possible owing to the presence of multiple timescale motions in the carboxy-terminal 30-40 residues of the *extended* PDZ1 and PDZ2 domains. Briefly, the width of the spectral density function reflects the fluctuations of the amide bond vector on different timescales with picosecond motions reported by elevated $J(0.87\omega_H)$, sub-nanosecond motions by depressed $J(\omega_N)$ and slower microsecond exchange term by $J(0)$ scaling rapidly with field strength [50].

Based on the above criterion for extracting an approximate timescale for internal motions, the elevated profile of $J(0.87\omega_H)$ values along the backbone of apo $PDZ1^{120}$ in the mobile loops (β2-β3 and α2-β6) and disordered termini, show the presence of picosecond motions (**Figure 7A)**. Slower microsecond motions were detected in the extended region between α1 and β4 as indicated by the higher than average $J(0)$ values (**Supplementary Figure 4A**). The flexibility of the loops has important implications for the configurational rearrangement of the binding site triggered by the bound ligand in $PDZ1^{120}$. In the HLG extension, both $J(0.87\omega_H)$ and $J(0)$ values deviate significantly from the average, but $J(\omega_N)$ remains constant (**Supplementary Figure 3A**). This trend reflects a dynamic secondary structure with fast picosecond motions in the presence of much slower conformational exchange in the microsecond regime (**Figure 7C**). The contribution of the exchange term in $J(0)$ is reflected by the rapid scaling of the values at higher field (**Supplementary Figure 4A**).

In $PDZ2^{270}$, the nearly uniform relaxation profiles at the three frequencies of motions suggest limited mobility in structured regions with the exception of fast picosecond motions in the flexible β2-β3 loop and the termini (**Figures 7D-7E and Supplementary Figures 3B & 4B**).

Effects of ligand binding on the dynamics of PDZ1 and PDZ2

In the ligand binding site of the PDZ1^{120} domain, the overall trend of $J(0.87\omega_H)$ remains unchanged with the exception of increased flexibility in the β2-β3 loop (**Figure 7A**). The rapid transverse relaxation rates (>20 Hz) of residues along the β2 strand (residues 25-30) could not be measured by traditional CPMG experiments in the complex [53]. The increased mobility of the β2-β3 loop coupled to the movement of the α2-helix in the complex suggests this strand may be responsible for a more flexible binding mode. Although the protein is effectively saturated (>99%) at a protein:peptide ratio of 1:1.3 with a sub-micromolar dissociation constant, the contribution of chemical exchange cannot be ruled out entirely. The large amide chemical shift difference (**Supplementary Figure 2A**) when compounded to relatively slow K_{on} [25; 54] can result in non-negligible R_{ex} terms [55; 56].

In the HLG subdomain, the systematic increase in $J(0.87\omega_H)$ values along the α3-α4 helices (**Figure 7A)** is accompanied by selective broadening of amide resonances (Thr9, Val91, Leu102, Gln105) in the hydrophobic core (**Figure 7B**). The presence of ligand has no effect on sharpening the amide resonances of residues (Val106-Leu110) from the dynamic α3-α4 extended loop which remains spectroscopically invisible. Thus, binding of ligand triggers a conformational transition in the dynamic HLG structure, which essentially becomes even more floppy in the complex.

The backbone dynamics of the peptide bound PDZ2^{270} domain is not perturbed compared to the free-state, with the exception of the flexible β2-β3 loop whose fast picosecond motions are quenched in the complex (**Figure 7D**). Thus, the ligand binding cleft has restricted mobility along the backbone in PDZ2 domain with greater flexibility in the PDZ1 domain. A significant difference between the two domains is observed in the flexible HLG extension from the PDZ1^{120} structure. Unlike the compact PDZ2^{270} structure, the HLG subdomain in PDZ1^{120} is dynamic sampling motions on multiple timescales. Most importantly, the conformational dynamics in the remote HLG structure in PDZ1^{120} is not quenched, but exacerbated by ligand binding through a long-range allosteric mechanism.

DISCUSSION

The structural and functional versatility of multi-PDZ domains plays a central role in cell signaling, including the assembly and turnover of macromolecular complexes [57; 58; 59; 60]. In this study, we have focused on determining the distinct structural mechanisms employed by the tandem PDZ domains of NHERF1 to differentiate between biological targets. Our NMR structures reveal that the putative PDZ1 and PDZ2 domains of NHERF1 are both stabilized by a novel carboxy-terminal HLG subdomain, through long-range hydrophobic and electrostatic interactions. The improved binding capability of these *extended* PDZ domains illustrate the importance of the distal structural appendages in regulating the activity of the binding site remotely [14]. Owing to high sequence homology between canonical PDZ domains, frequently the presence variable structures at the termini are overlooked. Our results substantiate an emerging theme that the sequence and structural propensity beyond the canonical PDZ domains are remarkably diverse and critical for mediating PDZ function [4; 61; 62; 63; 64; 65].

The Type 1 PDZ-binding motif in the CFTR-C peptide, shares a common binding mode in both PDZ1^{120} and PDZ2^{270} concurrent with previous findings [3;30]. The peptide augments the β-structure of the PDZ scaffold in an extended configuration. The carboxyl-terminal Leu^{0} embedded in a hydrophobic cleft between β2-α2 forms the crucial locus of hydrogen bonds, anchoring the peptide to the exposed backbone of the β1-β2 loop reinforced by a second and equally important H-bond pair coupling Thr^{-2} Oγ1 with His72 Nδ2 in PDZ1 and His212 Nδ2 in PDZ2. The charged (Arg^{-1} and Asp^{-2}) residues from the Type 1 motif are secured by distinct salt bridges to complementary side-chains from the β2-β3 strand and α1 helix in the binding site.

In the PDZ1^{120} binding site, the single H-bond between Glu^{43} (α1) and Arg^{-1} contributes significantly to the overall affinity, which is reinforced by the weak association between the triad of charged side-chains Asp^{-3}, His27 (β2) and Arg40 (β3). In PDZ2^{270}, the impact of natural sequence variation at the corresponding positions (Glu43->Asp183 and His27->Asn167) drastically lowers the affinity for the short peptide. Hence, differences in sequence at the binding site in PDZ1 and PDZ2 facilitate *unique electrostatic contacts* within each domain that modulates the generic affinity encoded by the buried carboxyl terminus. Nevertheless, PDZ2^{270} recovers its binding affinity for the longer, C-terminal domain from CFTR suggesting secondary interactions extending beyond the typical pentapeptide are equally important (**Table 1**). Indeed, our NMR based chemical shift perturbation maps uncovered the negatively charged upstream sequence from the long CFTR-C domain interacts favorably with a positively charged β2-β3 loop. The PDZ2 domain illustrates the length of the target peptide and its ability to complement the electrostatic charge of the flexible β2-β3 loop are important factors in mediating ligand recognition [66; 67] and the putative binding site may extend beyond the canonical structure [63].

To gain further insight into the broad specificity of the PDZ1 compared to PDZ2 domain, we applied a bioinformatics based approach to calculate the probabilities of amino acids at a particular position along the target peptide in each complex. The results of the analysis revealed distinct preferences for the penultimate side-chain of the peptide at the PDZ1 and PDZ2 binding sites respectively. In the PDZ1 domain, the P^{-1} pocket can accommodate either charged or hydrophobic residues with comparable probabilities, but the corresponding binding pocket of PDZ2^{270} favors a polar residue. The penultimate residue in the PDZ binding motif is known to be vital for tuning the binding affinities and this conclusion was also borne by our mutational studies [33]. Hence the PDZ1 domain has relatively high affinity for most Type 1 motifs. In PDZ2 domain, the high-affinity of binding to the longer CFTR carboxy-terminal tail illustrates, other factors such as the electrostatic charge of the upstream sequence are likely to be more important for certain targets.

Allosteric Effects in extended PDZ domains

Specificity in molecular recognition is frequently a close collaboration of the unique features of the sequence moderated by dynamic allostery in protein structures [68; 69]. The allosteric network of PDZ domains [70] has been widely discussed as a model for dynamic intramolecular communication between the primary scaffold and remote structural elements [40; 61; 71]. Frequently the absence of ligand induced conformational change in the

immediate binding site of PDZ domains masks detectable changes in the molecular motions along the backbone and side-chains at remote sites [36; 55; 61; 71].

In the presence of ligand, the PDZ domains of NHERF1 undergo distinct conformational and dynamic changes underscoring a fundamental difference in the mechanism of ligand recognition. The malleability of the *extended* PDZ1 domain facilitates both structural and dynamic changes invoking the classic induced fit model for ligand binding. The binding scaffold reorganized by the movement of α2 helix and the flexible β2-β3 loop is necessary to sterically adapt to the side-chains of Leu^{0} and Thr^{-2} from the peptide. Similar conformational changes have been observed in PDZ2 from the tyrosine phosphatase PTP-BL [72] and other systems [54; 73]. In fact the analysis of tertiary couplings in various PDZ domains has shown the conformational flexibility of the α2-helix offers a selective mechanism for allosteric regulation in ligand binding [74]. Since the extended PDZ1 structure is not modular, potential pathways for allosteric communication also exist between the ligand binding and the distal surface. The cooperative long range interactions mediated by clusters of residues propagate the conformational transformation triggered within the active site to a pliable C-terminal structure that consequently becomes even more dynamic.

Aside from aiding an adaptable mode of target recognition, the ligand induced conformational dynamics are also expected to modulate the entropic contribution to binding affinity [75; 76]. Several studies have demonstrated that the association of the PDZ domains with peptides is mainly enthalpy driven with a variable entropic contribution [43; 61; 77; 78]. Despite the small size of the ligand, the relatively strong H-bonds consistently reproduce the enthalpy change in the 2-7 kcal/mol range in most PDZ domains including NHERF1 [43]. The net entropy change is a summation of the favorable contribution from desolvation and loss of configurational entropy at the binding site [78]. The alterations in the binding site of $PDZ1^{120}$, necessitates a tunable mechanism to dissipate any negative entropy of binding facilitated by dynamic allostery observed in the floppy C-terminal structure. Thus the HLG module contributes favorably to the overall target affinity but the positive enhancement is arguably small for the isolated domain. In view of recent evidence from disease related mutations located specifically in the helical extension and the linker region [48], any ligand induced flexibility may be critical for the configuration of the tandem PDZ domains in NHERF1 [18; 37].

By contrast, the $PDZ2^{270}$ structure presents an almost rigid and pre-organized scaffold to the ligand with minimal structural rearrangement in the HLG module and little evidence for long-range dynamic allostery. The absence of ligand induced conformational changes belies the dramatic impact of the *extended* PDZ2 structure on binding affinity. Despite structural homology with PDZ1, the canonical PDZ2 domain is thermodynamically unstable. The notion of allostery in a structured network of interactions has been revised recently to include numerous examples of binding induced folding in intrinsically disordered domains [79; 80]. In the case of PDZ2 domain, the corresponding energetic cost of binding coupled to folding is presumably prohibitive resulting in drastically reduced affinity for small peptides (**Table 1**). The extended structure mediates the stability of the canonical binding site allosterically, and hence does not have to pay this thermodynamic penalty. Therefore, CFTR-C has much higher affinity for the extended $PDZ2^{270}$ domain. Evidently

the absence of plasticity in the binding site limits further its ability to adapt to non-standard sequences with debilitated affinity. A hypothetical question worth further investigation is whether it is possible to regulate ligand affinity through conformational changes in the HLG motif triggered by altered physiological conditions or phosphorylation state [91].

In conclusion, we have uncovered distinct mechanisms of structural and dynamic allostery in the *extended* PDZ1 and PDZ2 domains from NHERF1 that have important implications for target affinity and the configuration of the modular scaffold of NHERF1 [37]. A dynamic structure coupled with favorable binding site sequence, are the two most important factors responsible for the functional diversity of the PDZ1^{120} domain.

These findings have important implications for other members of the NHERF family of proteins as well. Frequently the structural synergy of multi PDZ domains reinforces the activity of the isolated scaffold and critical for transmitting long range signals along an adaptable binding platform [2; 81]. Further studies are necessary to elucidate the link between conformational changes in the individual PDZ domains of NHERF1 and its ability to sequester and release binding partners in supra-molecular assemblies.

Materials and Methods

Protein expression and purification

The human cDNA encoding NHERF1 PDZ1^{120} (residues 11-120) and PDZ2^{270} (residues 150-270) domains were subcloned into the pET151/D-TOPO vector (Invitrogen). The human cDNA encoding carboxy-terminal residues 1411-1480 from CFTR was subcloned into the pET151/D-TOPO vector (Invitrogen) or pET32a vector (Novagen). The proteins were expressed in Rosetta 2 (DE3) competent cells (EMD Biosciences) at 37°C and purified on a Ni^{2+} chelating column followed by gel filtration using a Superdex 200 10/300 GL column (GE Life Sciences). The affinity tags of the purified proteins were cleaved by AcTEV Protease (Invitrogen) before gel filtration purification.

Uniformly $^{15}N/^{13}C$ enriched proteins, were expressed in M9-minimal medium containing $^{15}NH_4Cl$ (Cambridge Isotope Laboratories) and [$^{13}C6$] glucose as sole nitrogen and carbon source, respectively. Unlabeled peptide (QDTRL) was purchased from GenScript. All NMR samples were prepared in a buffer containing 20 mM Tris at pH 7.5, 150 mM NaCl, 0.5 mM dithiothreitol, 0.5 mM EDTA and 90%H_2O/10% D_2O. Protein concentration was determined from the molar extinction coefficient at 280 nm and typically ranged from 300 to 400 μM. Protein-protein and protein peptide complexes were typically prepared by mixing $^{13}C/^{15}N$-labeled protein with unlabeled partner at slightly more than 1:1 molar ratio. The larger PDZ complexes with intact CFTR-C domain were mixed and co-purified over a sizing column.

NMR Spectroscopy

The NMR data were acquired at 15°C on Bruker *AVANCE* spectrometers equipped with TCI/TXI CryoProbes™ at field strengths ranging from 500-900 MHz. A standard suite of backbone and side-chain experiments were employed for chemical shift assignment of the isolated PDZ1^{120} and PDZ2^{270} domains and their respective complexes with the peptide and

the CFTR-C domain [82; 83] . Distance restraints required for structure calculations were obtained from 100 ms mixing time ^{15}N-edited and ^{13}C-edited 3D-NOESY-HSQC (aliphatic and aromatic region) spectra supplemented by 4D-(C^{13}, N^{15}) HSQC-NOESY-HSQC and 4D-(C^{13}, C^{13}) HSQC-NOESY-HSQC spectra. The bound peptide was assigned using 2D-^{15}N,^{13}C f_1, f_2-filtered NOESY datasets acquired at 900 MHz . Intermolecular NOEs were obtained from 2D-^{15}N,^{13}C f_2-filtered NOESY and 3D-^{15}N,^{13}C f_1-filtered ^{13}C/^{15}N-edited NOESY-HSQC experiment recorded with 100 ms mixing time.

The laboratory frame R_1, R_2 and ^{1}H-^{15}N NOE relaxation spectra were recorded according to established methods [84] at 15°C and two field strengths (500 and 900 MHz). To minimize systematic error, the relaxation experiments were acquired in an interleaved manner with the variable relaxation delays ranging between 0.02-1 s for R_1 measurements and 0.016-0.150s for R_2 measurements. Several time points were repeated to estimate the error in the intensity measurements. A 5s recycle delay with 3s saturation was used in the heteronuclear ^{1}H-^{15}N NOE experiments. The data were processed in NMRPipe [85] and analysed using NmrViewJ 8.0.3 [86]. The reduced spectral densities were calculated using published equations [51] and the errors propagated from the uncertainty in the relaxation measurements.

Structure Calculations

The NMR data were processed in Topspin 2.1 from Bruker Biospin and analyzed in CARA1.5 [87]. Three independent structures were calculated including those of apo PDZ1 domain and the ligand bound complexes of PDZ1^{120} and PDZ2^{270} domains respectively. The NOESY crosspeaks were assigned with the assistance of CANDID routine implemented in CYANA 2.1 [88]. The final ensemble of 1000 structures was generated with water refinement in ARIA 2.2 and CNS 1.5 forcefield [89]. Based on the lowest energies, the 20 best structures were selected and further analyzed in PROCHECK_NMR [92] for violations. The structural statistics of the ensemble of 20 best structures is reported in Table 2 along with the PDB and BMRB submission codes respectively.

Surface Plasmon Resonance

The SPR experiments were performed on Biacore X100 (GE Healthcare Life Sciences, NJ) at 15°C. The hydrogel matrix of the CM5 Biosensor chip (GE Healthcare Life Sciences, NJ) was activated by N-hydroxysuccinimide (NHS) and 1-ethyl-3-(3-dimethylaminopropyl) carbodiimide hydrochloride (EDC) (GE Healthcare Life Sciences, NJ). The activated surface was coated with a 10μg/ml solution of the ligand, a 70-residue carboxy-terminal fragment of CFTR dissolved in 10 mM sodium acetate at pH 5.2. The target immobilized ligand level (RU) was calculated according to the formula:

$$\text{Analyte binding capacity}\quad (RU) = (\text{analyte MW}/\text{ligand MW}) \times \text{immobilized ligand level}\quad (RU)$$

where MW is the molecular weight. One hundred RU was used as an optimal analyte binding capacity. Free ligand was washed away and the uncoated sites blocked by 1 M ethanolamine at pH 8.5. The analytes (*wildtype* or mutant PDZ1^{120}) were dissolved in HBS-EP buffer containing 10 mM HEPES buffer at pH 7.4, 150 mM NaCl, 3 mM EDTA, and 0.005% surfactant polysorbate 20. The analyte was injected at a series of concentrations

over the C-CFTR-coated surfaces at 30μl/min for 180 seconds. At the end of each injection, the sensor chip was regenerated with 4.0 M MgCl2, 50 mM triethylamine at pH 9.15 and washed with HBS-EP buffer.

Circular Dichroism Experiments

All protein samples of PDZ1 were dialyzed against 20 mM phosphate buffer at pH 7.5 with 150 mM NaCl and 1 mM DTT after purification. The protein concentration was measured at 280 nm using an extinction coefficient of 2980 $M^{-1}cm^{-1}$. CD experiments were performed on JASCO J-180 circular dichroism spectropolarimeter. For thermal denaturation, PDZ1 solution was diluted to a concentration of 0.3 mg/ml. Ellipticity was measured at a wavelength of 222 nm with a bandwidth of 1.0 nm, temperature dead band of 0.15°C, temperature equilibration time of 1.0 min, and averaging time of 2.0 s. Temperature scans were performed from 20°C to 70°C in 2°C steps.

Supplementary Material

Refer to Web version on PubMed Central for supplementary material.

Acknowledgments

NMR studies were supported by NIH GM-66354, and the 900 MHz system was purchased with funds from this grant, the Keck Foundation, and the member institutions of NYSBC. This work was supported by NIH R01 HL086496 (ZB), R01 GM047021 (DC), and 2G12 RR003060 from the National Center for Research Resources to CCNY.

Abbreviations

CBL	Carboxylate Binding Loop
CD	Circular Dichroism
CFTR	cystic fibrosis transmembrane regulator
CFTR-C	carboxy-terminal domain of CFTR
CPMG	Carr-Purcell-Meiboom-Gill
CT	a disordered carboxy-terminal domain of NHERF1
EBD	ERM binding domain
ERM	ezrin/radixin/moesin
FERM	4.1 and ERM
HLG	helix-loop-(3_{10}) helix motif
HSQC	heteronuclear single-quantum coherence
PDZ	postsynaptic density 95/disk-large/zonula occluden-1
PKC	Protein Kinase C
PTH1R	Parathyroid Hormone Type 1 Receptor

NHERF	Sodium/Hydrogen Exchange Regulatory Cofactor 1
NHE-3	Sodium/Hydrogen Exchange Type 3
NMR	Nuclear Magnetic Resonance

REFERENCES

1. Harris BZ, Lim WA. Mechanisms and role of PDZ domains in signalling complex assembly. J. Cell. Sci. 2001; 114:3219–3231. [PubMed: 11591811]
2. Zhang M. Scaffold proteins as dynamic switches. Nat. Chem. Biol. 2007; 3:756–757. [PubMed: 18007646]
3. Doyle DA, Lee A, Lewis J, Kim E, Sheng M, MacKinnon R. Crystal structures of a complexed and peptide-free membrane protein-binding domain: molecular basis of peptide recognition by PDZ. Cell. 1996; 85:1067–76. [PubMed: 8674113]
4. Tochio H, Mok YK, Zhang Q, Kan HM, Bredt DS, Zhang M. Formation of nNOS/PSD-95 PDZ dimer requires a preformed beta-finger structure from the nNOS PDZ domain. J. Mol. Biol. 2000; 303:359–370. [PubMed: 11031113]
5. Gallardo R, Ivarsson Y, Schymkowitz J, Rousseau F, Zimmermann P. Structural diversity of PDZ-lipid interactions. Chembiochem. 2010; 11:456–467. [PubMed: 20091728]
6. Weinman EJ, Hall RA, Friedman PA, Liu-Chen LY, Shenolikar S. The association of NHERF adaptor proteins with g protein-coupled receptors and receptor tyrosine kinases. Annu Rev Physiol. 2006; 68:491–505. [PubMed: 16460281]
7. Seidler U, Singh AK, Cinar A, Chen M, Hillesheim J, Hogema B, Riederer B. The role of the NHERF family of PDZ scaffolding proteins in the regulation of salt and water transport. Ann N Y Acad Sci. 2009; 1165:249–60. [PubMed: 19538313]
8. Blaine J, Weinman EJ, Cunningham R. The regulation of renal phosphate transport. Adv Chronic Kidney Dis. 2011; 18:77–84. [PubMed: 21406291]
9. LaLonde DP, Garbett D, Bretscher A. A regulated complex of the scaffolding proteins PDZK1 and EBP50 with ezrin contribute to microvillar organization. Mol Biol Cell. 2010; 21:1519–29. [PubMed: 20237154]
10. Reczek D, Berryman M, Bretscher A. Identification of EBP50: A PDZ-containing phosphoprotein that associates with members of the ezrin-radixin-moesin family. J Cell Biol. 1997; 139:169–79. [PubMed: 9314537]
11. Li J, Dai Z, Jana D, Callaway DJ, Bu Z. Ezrin controls the macromolecular complexes formed between an adapter protein Na+/H+ exchanger regulatory factor and the cystic fibrosis transmembrane conductance regulator. J Biol Chem. 2005; 280:37634–43. [PubMed: 16129695]
12. Morales FC, Takahashi Y, Momin S, Adams H, Chen X, Georgescu MM. NHERF1/EBP50 head-to-tail intramolecular interaction masks association with PDZ domain ligands. Mol Cell Biol. 2007; 27:2527–37. [PubMed: 17242191]
13. Li J, Callaway DJ, Bu Z. Ezrin induces long-range interdomain allostery in the scaffolding protein NHERF1. J. Mol. Biol. 2009; 392:166–80. [PubMed: 19591839]
14. Bhattacharya S, Dai Z, Li J, Baxter S, Callaway DJ, Cowburn D, Bu Z. A conformational switch in the scaffolding protein NHERF1 controls autoinhibition and complex formation. J Biol Chem. 2010; 285:9981–94. [PubMed: 20042604]
15. Li J, Poulikakos PI, Dai Z, Testa JR, Callaway DJ, Bu Z. Protein kinase C phosphorylation disrupts Na+/H+ exchanger regulatory factor 1 autoinhibition and promotes cystic fibrosis transmembrane conductance regulator macromolecular assembly. J Biol Chem. 2007; 282:27086–99. [PubMed: 17613530]
16. Farago B, Li J, Cornilescu G, Callaway DJ, Bu Z. Activation of nanoscale allosteric protein domain motion revealed by neutron spin echo spectroscopy. Biophys J. 2010; 99:3473–82. [PubMed: 21081097]

17. Ardura JA, Friedman PA. Regulation of G protein-coupled receptor function by Na+/H+ exchange regulatory factors. Pharmacol. Rev. 2011; 63:882–900. [PubMed: 21873413]

18. Wang W, Weng J, Zhang X, Liu M, Zhang M. Creating conformational entropy by increasing interdomain mobility in ligand binding regulation: a revisit to N-terminal tandem PDZ domains of PSD-95. J. AM. Chem. Soc. 2009; 131:787–796. [PubMed: 19072119]

19. Wang B, Means CK, Yang Y, Mamonova T, Bisello A, Altschuler DL, Scott JD, Friedman PA. Ezrin-anchored protein kinase A coordinates phosphorylation-dependent disassembly of a NHERF1 ternary complex to regulate hormone-sensitive phosphate transport. J Biol Chem. 2012; 287:24148–63. [PubMed: 22628548]

20. Reczek D, Bretscher A. The carboxyl-terminal region of EBP50 binds to a site in the amino-terminal domain of ezrin that is masked in the dormant molecule. J Biol Chem. 1998; 273:18452–8. [PubMed: 9660814]

21. Hall RA, Ostedgaard LS, Premont RT, Blitzer JT, Rahman N, Welsh MJ, Lefkowitz RJ. A C-terminal motif found in the beta2-adrenergic receptor, P2Y1 receptor and cystic fibrosis transmembrane conductance regulator determines binding to the Na+/H+ exchanger regulatory factor family of PDZ proteins. Proc Natl Acad Sci U S A. 1998; 95:8496–8501. [PubMed: 9671706]

22. Wang S, Raab RW, Schatz PJ, Guggino WB, Li M. Peptide binding consensus of the NHE-RF-PDZ1 domain matches the C-terminal sequence of cystic fibrosis transmembrane conductance regulator (CFTR). FEBS Lett. 1998; 427:103–108. [PubMed: 9613608]

23. Riordan JR, Rommens JM, Kerem B, Alon N, Rozmahel R, Grzelczak Z, Zielenski J, Lok S, Plavsic N, Chou JL. Identification of the cystic fibrosis gene: cloning and characterization of complementary DNA. Science. 1989; 245:1066–73. [PubMed: 2475911]

24. Li C, Naren AP. Analysis of CFTR interactome in the macromolecular complexes. Methods Mol Biol. 2011; 741:255–70. [PubMed: 21594790]

25. Raghuram V, Mak DO, Foskett JK. Regulation of cystic fibrosis transmembrane conductance regulator single-channel gating by bivalent PDZ-domain-mediated interaction. Proc Natl Acad Sci USA. 2001; 98:1300–5. [PubMed: 11158634]

26. Swiatecka-Urban A, Duhaime M, Coutermarsh B, Karlson KH, Collawn J, Milewski M, Cutting GR, Guggino WB, Langford G, Stanton BA. PDZ domain interaction controls the endocytic recycling of the cystic fibrosis transmembrane conductance regulator. J Biol. Chem. 2002; 277:40099–105. [PubMed: 12167629]

27. Naren AP, Cobb B, Li C, Roy K, Nelson D, Heda GD, Liao J, Kirk KL, Sorscher EJ, Hanrahan J, Clancy JP. A macromolecular complex of beta 2 adrenergic receptor, CFTR, and ezrin/radixin/moesin-binding phosphoprotein 50 is regulated by PKA. Proc Natl Acad Sci U S A. 2003; 100:342–6. [PubMed: 12502786]

28. Favia M, Guerra L, Fanelli T, Cardone RA, Monterisi S, Di Sole F, Castellani S, Chen M, Seidler U, Reshkin SJ, Conese M, Casavola V. Na+/H+ exchanger regulatory factor 1 overexpression-dependent increase of cytoskeleton organization is fundamental in the rescue of F508del cystic fibrosis transmembrane conductance regulator in human airway CFBE41o- cells. Mol Biol Cell. 2010; 21:73–86. [PubMed: 19889841]

29. Shenolikar S, Weinman EJ. NHERF: targeting and trafficking membrane proteins. Am J Physiol Renal Physiol. 2001; 280:389–395.

30. Karthikeyan S, Leung T, Birrane G, Webster G, Ladias JA. Crystal structure of the PDZ1 domain of human Na(+)/H(+) exchanger regulatory factor provides insights into the mechanism of carboxyl-terminal leucine recognition by class I PDZ domains. J Mol Biol. 2001; 308:963–73. [PubMed: 11352585]

31. Karthikeyan S, Leung T, Ladias JA. Structural determinants of the Na+/H+ exchanger regulatory factor interaction with the beta 2 adrenergic and platelet-derived growth factor receptors. J Biol Chem. 2002; 277:18973–8. [PubMed: 11882663]

32. Elkins JM, Papagrigoriou E, Berridge G, Yang X, Phillips C, Gileadi C, Savitsky P, Doyle DA. Structure of PICK1 and other PDZ domains obtained with the help of self-binding C-terminal extensions. Protein Sci. 2007; 16:683–94. [PubMed: 17384233]

33. Tonikian R, Zhang Y, Sazinsky SL, Currell B, Yeh JH, Reva B, Held HA, Appleton BA, Evangelista M, Wu Y, Xin X, Chan AC, Seshagiri S, Lasky LA, Sander C, Boone C, Bader GD, Sidhu SS. A specificity map for the PDZ domain family. PLoS Biol. 2008; 6
34. Kim J, Kim I, Yang JS, Shin YE, Hwang J, Park S, Choi YS, Kim S. Rewiring of PDZ domain-ligand interaction network contributed to eukaryotic evolution. PLoS Genet. 2012; 8
35. Fuentes EJ, Der CJ, Lee AL. Ligand-dependent dynamics and intramolecular signaling in a PDZ domain. J Mol Biol. 2004; 335:1105–15. [PubMed: 14698303]
36. Walma T, Spronk CA, Tessari M, J. A, Schepens J, Hendriks W, Vuister GW. Structure, dynamics and binding characteristics of the second PDZ domain of PTP-BL. J. Mol. Biol. 2002; 316:1101–10. [PubMed: 11884147]
37. Long JF, Tochio H, Wang P, Fan JS, Sala C, Niethammer M, Sheng M, Zhang M. Supramodular structure and synergistic target binding of the N-terminal tandem PDZ domains of PSD-95. J. Mol. Biol. 2003; 327:203–214. [PubMed: 12614619]
38. Hillier BJ, Christopherson KS, Prehoda KE, Bredt DS, Lim WA. Unexpected modes of PDZ domain scaffolding revealed by structure of nNOS-syntrophin complex. Science. 1999; 284:812–5. [PubMed: 10221915]
39. Songyang Z, Fanning AS, Fu C, Xu J, Marfatia SM, Chishti AH, Crompton A, Chan AC, Anderson JM, Cantley LC. Recognition of Unique Carboxyl-Terminal Motifs by Distinct PDZ Domains. Science. 1997; 275:73–76. [PubMed: 8974395]
40. Gerek ZN, Ozkan SB. Change in allosteric network affects binding affinities of PDZ domains: analysis through perturbation response scanning. PLoS Comput Biol. 2011; 7
41. Ivarsson Y. Plasticity of PDZ domains in ligand recognition and signaling. FEBS Lett. 2012
42. Mostarda S, Gfeller D, Rao F. Beyond the binding site: the role of the β_2-β_3 loop and extra-domain structures in PDZ domains. PLoS Comput Biol. 2012; 8
43. Cushing PR, Fellows A, Villone D, Boisguerin P, Madden DR. The relative binding affinities of PDZ partners for CFTR: a biochemical basis for efficient endocytic recycling. Biochemistry. 2008; 47:10084–98. [PubMed: 18754678]
44. Chothia C, Lesk AM. The relation between the divergence of sequence and structure in proteins. EMBO J. 1986; 5:823–6. [PubMed: 3709526]
45. Karim Z, Gerard B, Bakouh N, Alili R, Leroy C, Beck L, Silve C, Planelles G, Urena-Torres P, Grandchamp B, Friedlander G, Prie D. NHERF1 Mutations and Responsiveness of Renal Parathyroid Hormone. N Engl J Med. 2008; 359:1128–1135. [PubMed: 18784102]
46. Karthikeyan S, Leung T, Ladias JA. Structural basis of the Na+/H+ exchanger regulatory factor PDZ1 interaction with the carboxyl-terminal region of the cystic fibrosis transmembrane conductance regulator. J Biol Chem. 2001; 276:19683–6. [PubMed: 11304524]
47. Moyer BD, Duhaime M, Shaw C, Denton J, Reynolds D, Karlson KH, Pfeiffer J, Wang S, Mickle JE, Milewski M, Cutting GR, Guggino WB, Li M, Stanton BA. The PDZ-interacting Domain of Cystic Fibrosis Transmembrane Conductance Regulator Is Required for Functional Expression in the Apical Plasma Membrane. J Biol Chem. 2000; 275:27069–74. [PubMed: 10852925]
48. Mamonova T, Kurnikova M, Friedman PA. Structural basis for NHERF1 PDZ domain binding. Biochemistry. 2012; 51:3110–20. [PubMed: 22429102]
49. Shenolikar S, Voltz JW, Cunningham R, Weinman EJ. Regulation of ion transport by the NHERF family of PDZ proteins. Physiology (Bethesda). 2004; 19:362–9. [PubMed: 15546854]
50. Peng JW, Wagner G. Mapping of the spectral densities of N-H bond motions in eglin c using heteronuclear relaxation experiments. Biochemistry. 1992; 31:8571–86. [PubMed: 1390643]
51. Farrow NA, Zhang O, Szabo A, Torchia DA, Kay LE. Spectral density function mapping using 15N relaxation data exclusively. J Biomol NMR. 1995; 6:153–62. [PubMed: 8589604]
52. Mandel AM, Akke M, Palmer AG 3rd. Backbone dynamics of Escherichia coli ribonuclease HI: correlations with structure and function in an active enzyme. J Mol Biol. 1995; 246:144–63. [PubMed: 7531772]
53. Loria JP, Rance M, Palmer AG. A Relaxation-Compensated Carr−Purcell−Meiboom−Gill Sequence for Characterizing Chemical Exchange by NMR Spectroscopy. JACS. 1999; 121:2331–2332.

54. Chi CN, Bach A, Engström A, Wang H, Strømgaard K, Gianni S, Jemth P. A sequential binding mechanism in a PDZ domain. Biochemistry. 2009; 48:7089–7097. [PubMed: 19496620]
55. Niu X, Chen Q, Zhang J, Shen W, Shi Y, Wu J. Interesting structural and dynamical behaviors exhibited by the AF-6 PDZ domain upon Bcr peptide binding. Biochemistry. 2007; 46:15042–53. [PubMed: 18052198]
56. Liu J, Zhang J, Yang Y, Huang H, Shen W, Hu Q, Wang X, Wu J, Shi Y. Conformational change upon ligand binding and dynamics of the PDZ domain from leukemia-associated Rho guanine nucleotide exchange factor. Protein Sci. 2008; 17:1003–14. [PubMed: 18411422]
57. Ackermann F, Zitranski N, Heydecke D, Wilhelm B, Gudermann T, Boekhoff I. The Multi-PDZ domain protein MUPP1 as a lipid raft-associated scaffolding protein controlling the acrosome reaction in mammalian spermatozoa. J Cell Physiol. 2008; 214:757–768. [PubMed: 17894389]
58. Feng W, Zhang M. Organization and dynamics of PDZ-domain-related supramodules in the postsynaptic density. Nature Reviews Neuroscience. 2009; 10:87–99.
59. Garbett D, Bretscher A. PDZ interactions regulate rapid turnover of the scaffolding protein EBP50 in microvilli. The Journal of Cell Biology. 2012; 198:195–203. [PubMed: 22801783]
60. Garbett D, LaLonde DP, Bretscher A. The scaffolding protein EBP50 regulates microvillar assembly in a phosphorylation-dependent manner. J Cell Biol. 2010; 191:397–413. [PubMed: 20937695]
61. Petit CM, Zhang J, Sapienza PJ, Fuentes EJ, Lee AL. Hidden dynamic allostery in a PDZ domain. Proc Natl Acad Sci U S A. 2009; 106:18249–54. [PubMed: 19828436]
62. Wang CK, Pan L, Chen J, Zhang M. Extensions of PDZ domains as important structural and functional elements. Protein Cell. 2010; 1:737–51. [PubMed: 21203915]
63. Chi CN, Haq SR, Rinaldo S, Dogan J, Cutruzzolà F, Engström Å, Gianni S, Lundström P, Jemth P. Interactions outside the boundaries of the canonical binding groove of a PDZ domain influence ligand binding. Biochemistry. 2012; 51:8971–8979. [PubMed: 23046383]
64. Wawrzyniak AM, Vermeiren E, Zimmermann P, Ivarsson Y. Extensions of PSD-95/discs large/ZO-1 (PDZ) domains influence lipid binding and membrane targeting of syntenin-1. FEBS Letters. 2012; 586:1445–1451. [PubMed: 22673509]
65. Luck K, Charbonnier S, Travé G. The emerging contribution of sequence context to the specificity of protein interactions mediated by PDZ domains. FEBS Letters. 2012; 586:2648–2661. [PubMed: 22709956]
66. Pegan S, Tan J, Huang A, Slesinger PA, Riek R, Choe S. NMR studies of interactions between C-terminal tail of Kir2.1 channel and PDZ1,2 domains of PSD95. Biochemistry. 2007; 46:5315–5322. [PubMed: 17437338]
67. Balana B, Maslennikov I, Kwiatkowski W, Stern KM, Bahima L, Choe S, Slesinger PA. Mechanism underlying selective regulation of G protein-gated inwardly rectifying potassium channels by the psychostimulant-sensitive sorting nexin 27. Proc Natl Acad Sci U S A. 2011; 108:5831–5836. [PubMed: 21422294]
68. Gunasekaran K, Ma B, Nussinov R. Is allostery an intrinsic property of all dynamic proteins? Proteins. 2004; 57:433–443. [PubMed: 15382234]
69. Kalodimos CG. Protein function and allostery: a dynamic relationship. Ann N Y Acad Sci. 2012; 1260:81–86. [PubMed: 22256894]
70. Lockless SW, Ranganathan R. Evolutionarily conserved pathways of energetic connectivity in protein families. Science. 1999; 286:295–9. [PubMed: 10514373]
71. Zhang J, Sapienza PJ, Ke H, Chang A, Hengel SR, Wang H, Phillips GN, Lee AL. Crystallographic and nuclear magnetic resonance evaluation of the impact of peptide binding to the second PDZ domain of protein tyrosine phosphatase 1E. Biochemistry. 2010; 49:9280–91. [PubMed: 20839809]
72. Gianni S, Walma T, Arcovito A, Calosci N, Bellelli A, Engström A, Travaglini-Allocatelli C, Brunori M, Jemth P, Vuister GW. Demonstration of long-range interactions in a PDZ domain by NMR, kinetics, and protein engineering. Structure. 2006; 14:1801–1809. [PubMed: 17161370]
73. Grembecka J, Cierpicki T, Devedjiev Y, Derewenda U, Kang BS, Bushweller JH, Derewenda ZS. The binding of the PDZ tandem of syntenin to target proteins. Biochemistry. 2006; 45:3674–3683. [PubMed: 16533050]

74. Ho BK, Agard DA. Conserved tertiary couplings stabilize elements in the PDZ fold, leading to characteristic patterns of domain conformational flexibility. Protein Sci. 2010; 19:398–411. [PubMed: 20052683]
75. Hilser VJ, Wrabl JO, Motlagh HN. Structural and energetic basis of allostery. Annu. Rev. Biophys. 2012; 41:585–609. [PubMed: 22577828]
76. Akke M. Conformational dynamics and thermodynamics of protein-ligand binding studied by NMR relaxation. Biochem Soc Trans. 2012; 40:419–423. [PubMed: 22435823]
77. Milev S, Bjelić S, Georgiev O, Jelesarov I. Energetics of peptide recognition by the second PDZ domain of human protein tyrosine phosphatase 1E. Biochemistry. 2007; 46:1064–78. [PubMed: 17240990]
78. Saro DLT, Rupasinghe C, Paredes A, Caspers N, Spaller MR. A thermodynamic ligand binding study of the third PDZ domain (PDZ3) from the mammalian neuronal protein PSD-95. Biochemistry. 2007; 46:6340–52. [PubMed: 17474715]
79. Luque I, Leavitt SA, Freire E. The linkage between protein folding and functional cooperativity: two sides of the same coin? Annu Rev Biophys Biomol Struct. 2002; 31:235–256. [PubMed: 11988469]
80. Hilser VJ, Thompson EB. Intrinsic disorder as a mechanism to optimize allosteric coupling in proteins. Proc Natl Acad Sci U S A. 2007; 104:8311–8315. [PubMed: 17494761]
81. Liu W, Wen W, Wei Z, Yu J, Ye F, Liu CH, Hardie RC, Zhang M. The INAD scaffold is a dynamic, redox-regulated modulator of signaling in the Drosophila eye. Cell. 2011; 145:1088–1101. [PubMed: 21703451]
82. Sattler M, Schleucher J, Greisinger C. Heteronuclear multidimensional NMR experiments for the structure determination of proteins in solution employing pulse field gradients. Prog. NMR Spectrosc. 1999; 34:93–158.
83. Cavanagh, J.; Fairbrother, WJ.; Palmer, AGI.; Skelton, NJ. Protein NMR spectroscopy : Principles and practice. Academic Press; San Diego: 1996. Protein NMR spectroscopy : Principles and practice (San Diego: Academic Press). (1996)..
84. Farrow NA, Muhandiram R, Singer AU, Pascal SM, Kay CM, Gish G, Shoelson SE, Pawson T, Forman-Kay JD, Kay LE. Backbone dynamics of a free and phosphopeptide-complexed Src homology 2 domain studied by 15N NMR relaxation. Biochemistry. 1994; 33:5984–6003. [PubMed: 7514039]
85. Delaglio F, Grzesiek S, Vuister GW, Zhu G, Pfeifer J, Bax A. NMRPipe: a multidimensional spectral processing system based on UNIX pipes. J Biomol NMR. 1995; 6:277–93. [PubMed: 8520220]
86. Johnson BA. Using NMRView to visualize and analyze the NMR spectra of macromolecules. Methods Mol Biol. 2004; 278:313–52. [PubMed: 15318002]
87. Keller, R. Optimizing the process of nuclear magnetic resonance spectrum analysis and computer aided resonance assignment. ETH; 2004.
88. Güntert P, Mumenthaler C, Wüthrich K. Torsion angle dynamics for NMR structure calculation with the new program DYANA. J. Mol. Biol. 1997; 273:283–298. [PubMed: 9367762]
89. Nilges M, Macias MJ, O'Donoghue SI, Oschkinat H. Automated NOESY interpretation with ambiguous distance restraints: the refined NMR solution structure of the pleckstrin homology domain from beta-spectrin. J Mol Biol. 1997; 269:408–22. [PubMed: 9199409]
90. Thompson JD, Gibson TJ, Higgins DG. Multiple sequence alignment using ClustalW and ClustalX. Curr Protoc Bioinformatics. 2002 Chapter 2, Unit 2 3.
91. Koradi R, Billeter M, Wuthrich K. MOLMOL: a program for display and analysis of macromolecular structures. J. Mol. Graphics. 1996; 14:51–55.
92. Pettersen EF, Goddard TD, Huang CC, Couch GS, Greenblatt DM, Meng EC, Ferrin TE. UCSF Chimera--a visualization system for exploratory research and analysis. J Comput Chem. 2004; 25:1605–12. [PubMed: 15264254]

- Novel helical extension exists in both PDZ1 and PDZ2 domains of NHERF1.
- The extended PDZ domains are more stable than the canonical structure
- Binding site sequence variation and difference in plasticity dictate PDZ binding affinity.
- PDZ1 is malleable with motions on multiple timescales, while PDZ2 is relatively rigid.
- Distinct ligand induced dynamic and structural allostery observed in the *extended* PDZ1 and PDZ2 domains.

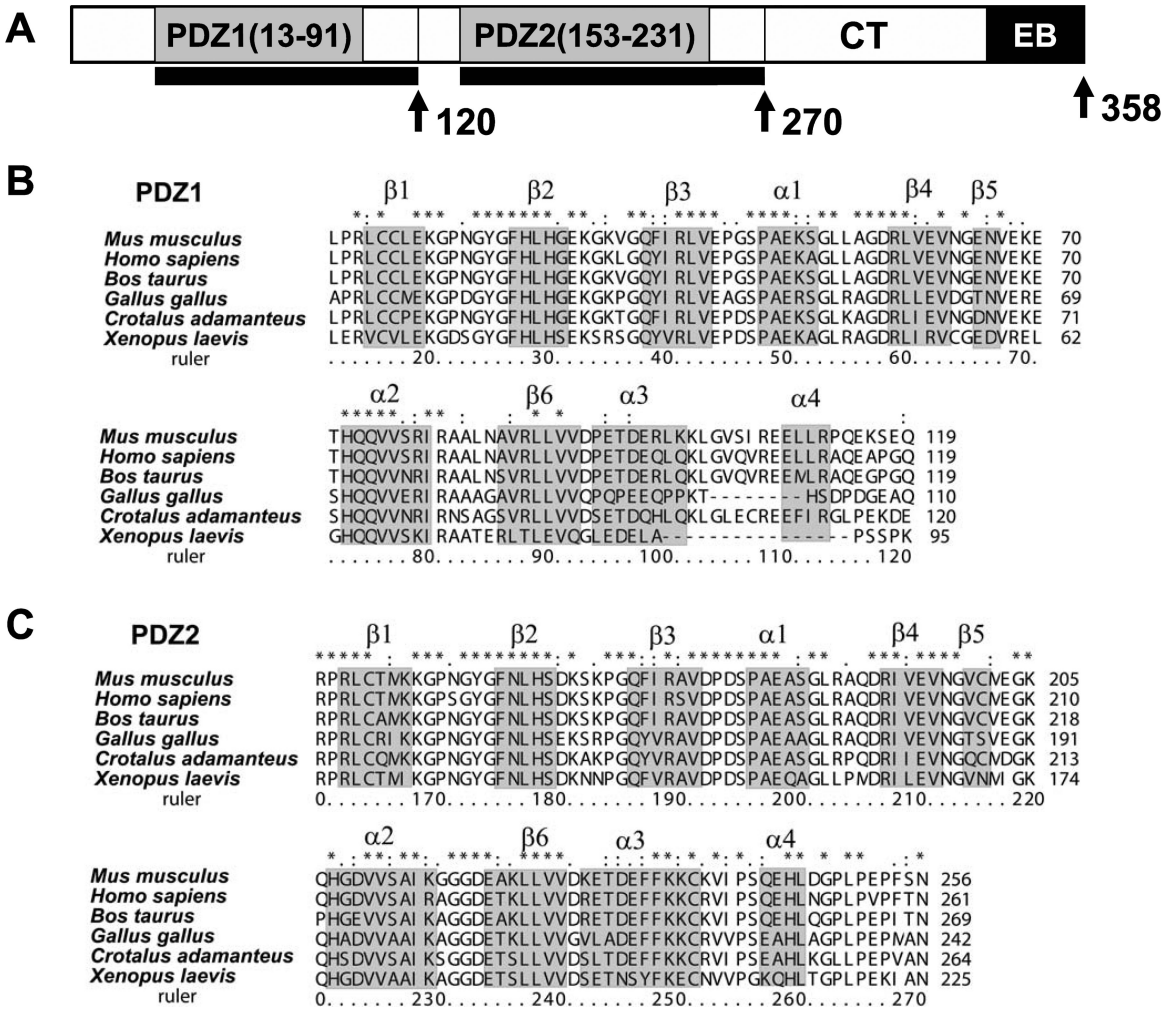

Figure 1. NHERF1 multiple sequence alignment

(A) Schematic representation of human NHERF1 consisting of tandem PDZ1 and PDZ2 domains with a mostly disordered carboxy-terminal (CT) domain. The CT domain has overlapping Ezrin-binding (EB) and PDZ-binding motifs. The lengths of the putative PDZ domains are indicated in the box and the *extended* structure by solid bars. **(B)** Multiple sequence alignment of PDZ1, and **(C)** PDZ2 domains of NHERF1 from various species generated by the program ClustalX [90]. The conserved sequence in secondary structure from the canonical domain is highlighted by grey boxes.

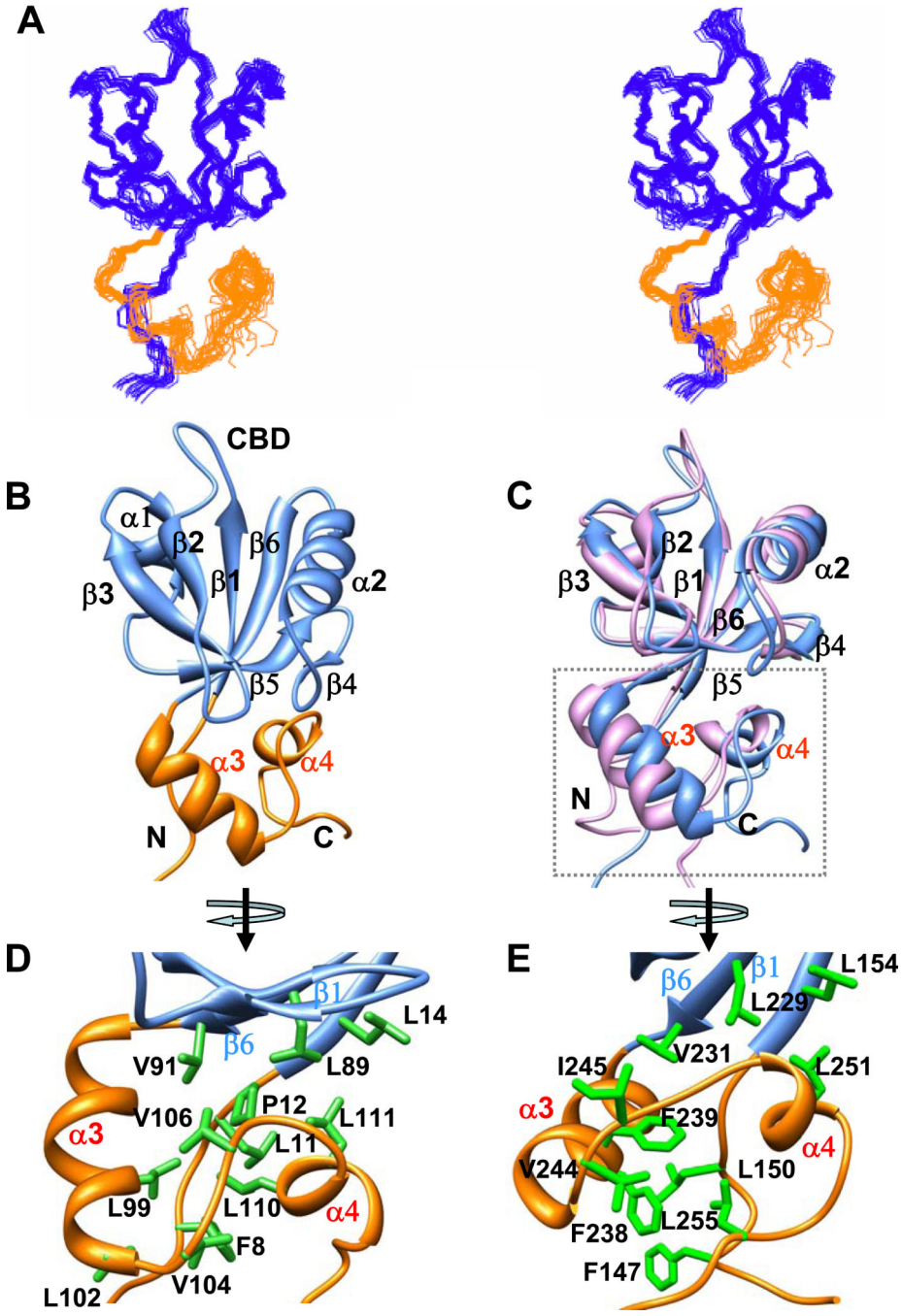

Figure 2. Structural comparison of PDZ1^{120} and PDZ2^{270} domains

(A) Stereoview of an ensemble of extended PDZ1^{120} structures determined by NMR with the canonical PDZ domain (residues 13-91) indicated in blue and the HLG subdomain in gold. **(B)** Backbone representation of PDZ1^{120} domain with annotated secondary structure. **(C)** Backbone superposition of the canonical domain from PDZ1^{120} (blue, residues 13-91) and PDZ2^{270} (pink, residues 153-231). The corresponding RMSD of 0.95 Å is significantly worse with RMSD of 1.5 Å when the HLG extensions are included in the alignment. The unstructured amino- and carboxy-termini residues were excluded from the figure. **(D)**

Hydrophobic and aliphatic side-chain contacts (green sticks) in the HLG extension from PDZ1^{120}, and **(E)** PDZ2^{270} domain.

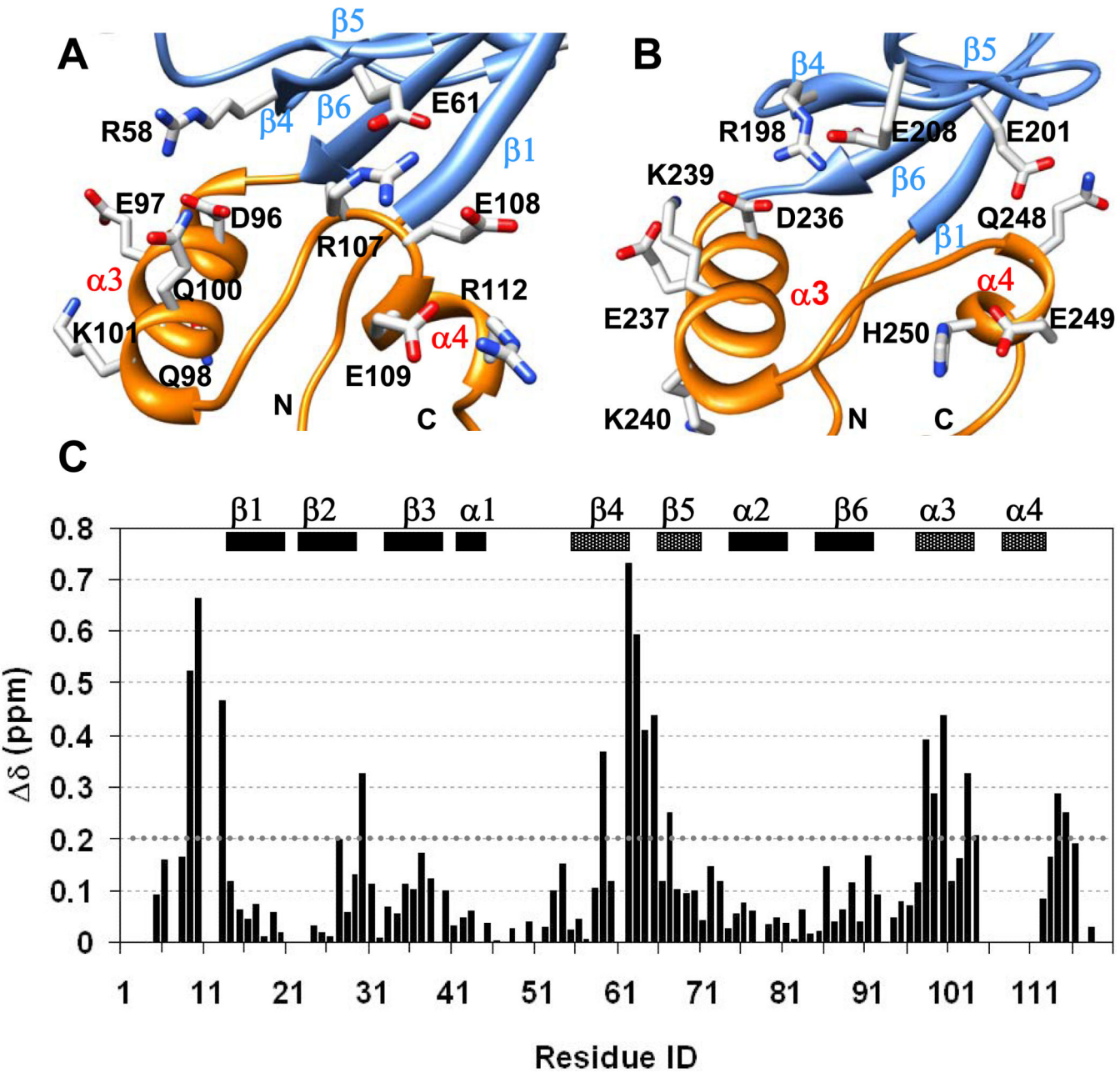

Figure 3. Overview of electrostatic interactions in the HLG subdomains.

(A) Intra-helical and long-range electrostatic interactions involving charged and polar side-chains in PDZ1^{120}, and (**B**) PDZ2^{270} domain represented by sticks color coded by type of heteroatom. **(C)** Chemical shift difference plot between *wildtype* PDZ1^{120} domain and the Glu61->Gly61 mutant at 15°C. The weighted difference was calculated using the relation $\Delta \sqrt{((\delta H^N)^2 + (\delta N/5)^2)}$. The N-terminal residues and secondary structure (β4, β5, α3 and α4) with significant chemical shift perturbation (>0.2 ppm, dotted line) in the mutant protein are indicated by different box pattern.

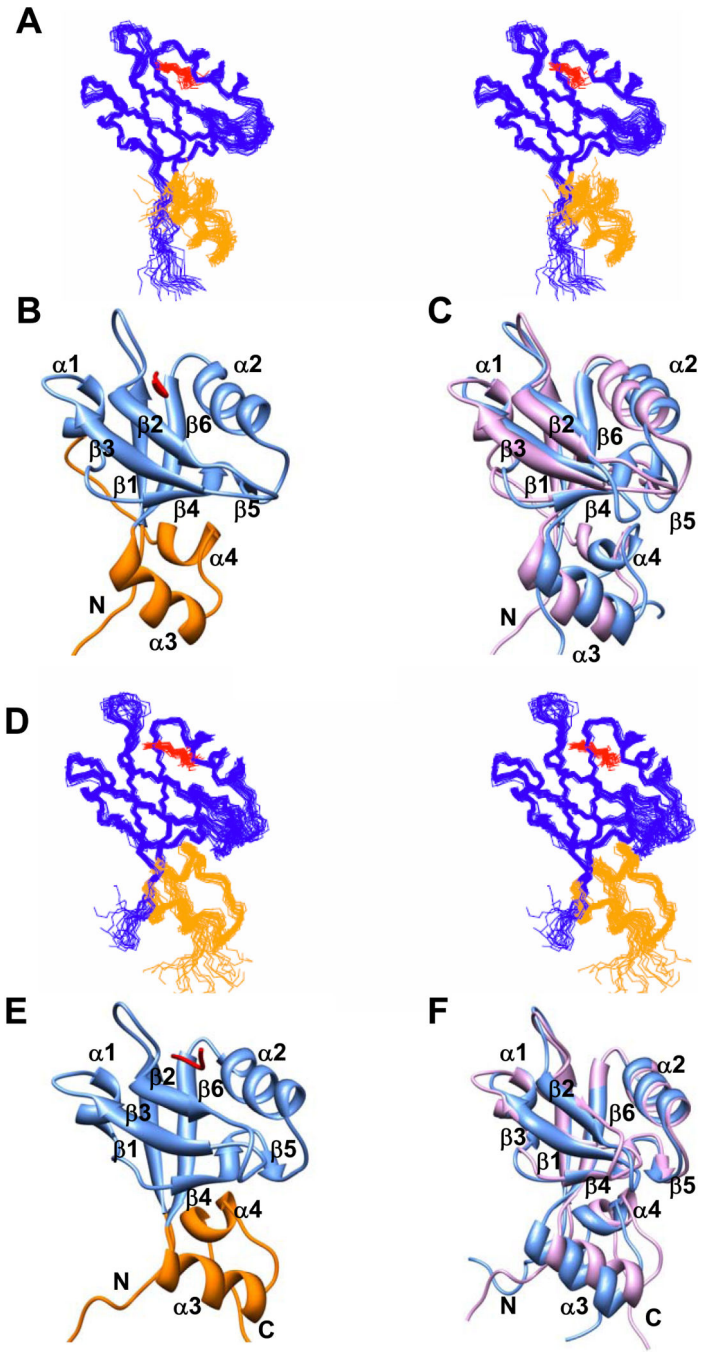

Figure 4. CFTR-C peptide (QDTRL) bound PDZ1^{120} and PDZ2^{270} structures

(A) Stereoview of the ensemble of 20 best NMR structures of PDZ1^{120} in complex with CFTR-C peptide (red). **(B)** Ribbon representation of single PDZ1^{120} complex structure. **(C)** Backbone superposition of PDZ1 canonical domain (residues 13-91) in the presence (pink) and absence of peptide (blue). The corresponding backbone RMSD (13-91) of 1.7 Å increases to 1.9 Å when additional residues (13-110) from the HLG subdomain are included in the alignment. **(D)** Stereoview of the CFTR-C peptide (red) bound PDZ2^{270} complex structure. **(E)** Ribbon representation of single PDZ2^{270} complex structure. **(F)** Backbone

superposition of PDZ2 canonical domain (residues 153-231) in the presence (pink) and absence of peptide (blue). The corresponding backbone RMSD (153-231) of 1.0 Å increases to 1.2 Å when residues (153-252) from the HLG subdomain are included in the alignment. The stereoviews were generated in MOLMOL 2.1 [91] and ribbons using UCSF Chimera package [92].

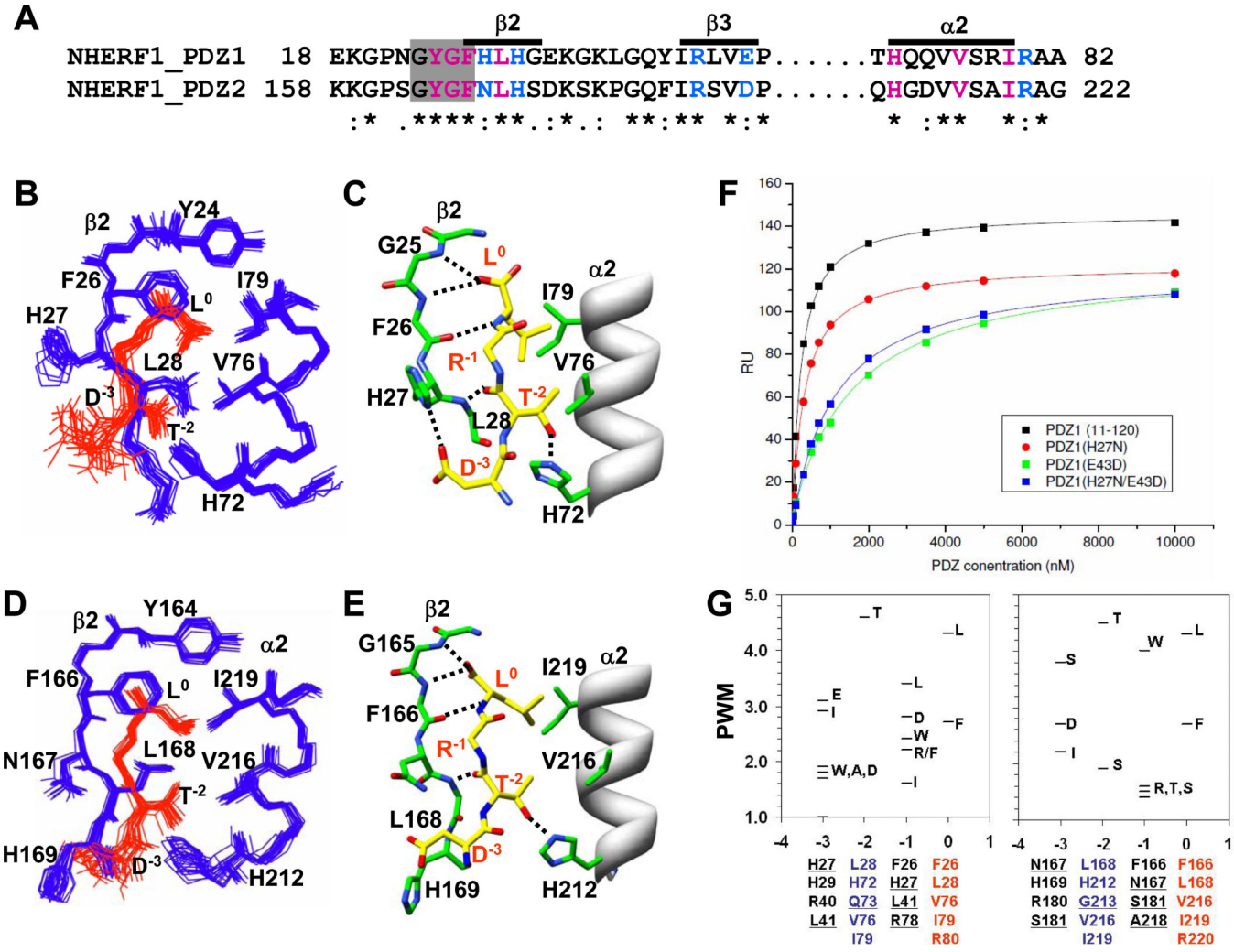

Figure 5. Overview of intermolecular interactions in the PDZ1 and PDZ2 peptide complexes

(A) Partial sequence alignment of the binding site residues from PDZ1 and PDZ2 domains color-coded based on hydrophobic (magenta), H-bond (magenta), and variable electrostatic (blue) interactions. Residues in the carboxylate binding loop are highlighted by the grey box. **(B)** Structural ensemble of PDZ1^{120} (blue) binding site with CFTR-C peptide (red), and **(C)** the corresponding intermolecular H-bonds (dotted lines) in a single structure. As per established convention for annotating PDZ-binding motifs, the carboxy-terminal residue of the CFTR-C peptide is '0' and the amino-terminal Asp is '-3' [3]. For visual clarity the side-chain of Arg^{-1} is not shown in the figure. **(D)** Structural ensemble of PDZ2^{270} (blue) binding site with CFTR-C peptide (red), and **(E)** the corresponding intermolecular H-bonds (dotted lines) in a single structure. **(F)** Binding curves of CFTR-C domain with *wildtype* and mutant PDZ1^{120} domains from SPR measurements with the affinities reported in Table 1. **(G)** Graphical representation of the position weight matrix (PWM) of amino acid propensities at various positions (0 to -3) along the Type 1 PDZ motif calculated using published protocol with details provided in Supplementary Material [34]. PWM reported along the Y-axis is effectively the logarithm of probabilities and hence no units are required. Residues

associated with each binding pocket identified from sequence alignment are listed below the plot with the natural mutations underlined.

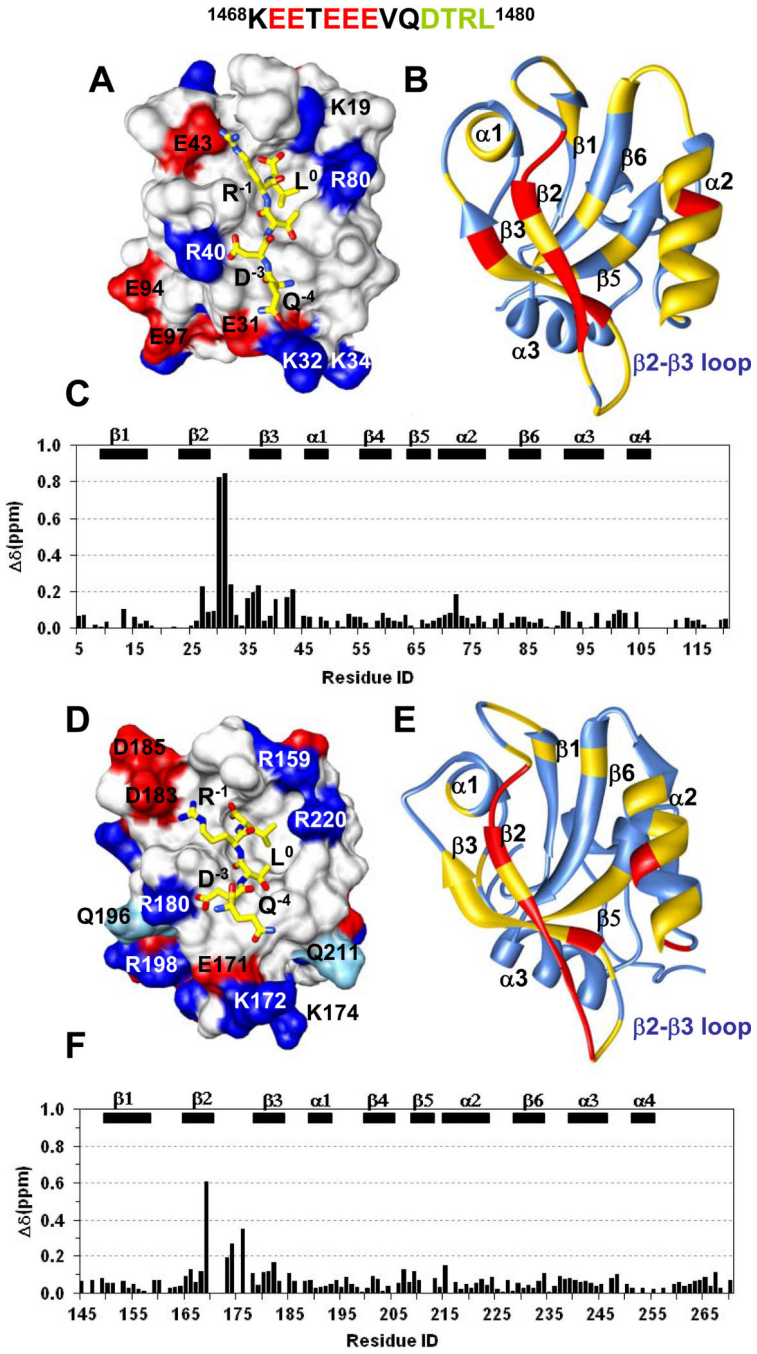

Figure 6. Electrostatic complementarity at peptide/protein complex interface

(A) The annotated electrostatic binding surface of PDZ1^{120} with peptide (yellow) showing charged side-chain interactions. **(B)** Chemical shift perturbation of PDZ1^{120} bound to CFTR-C domain painted yellow (>0.2 ppm) and red (>1.00 ppm) on the ribbon representation of the protein backbone. **(C)** The weighted difference in amide chemical shifts between the peptide and the CFTR-C domain bound to PDZ1^{120}. **(D)** The annotated electrostatic surface of PDZ2^{270} with bound peptide (yellow) showing charged side-chain interactions. Polar residues (cyan) at the binding site with significant chemical shift

perturbation are also labeled. **(E)** Chemical shift mapping of the CFTR-C binding site of $PDZ2^{270}$ domain using identical cutoffs described above for panel (B). **(F)** The weighted difference in amide chemical shifts between the peptide and CFTR-C domain bound to $PDZ2^{270}$.

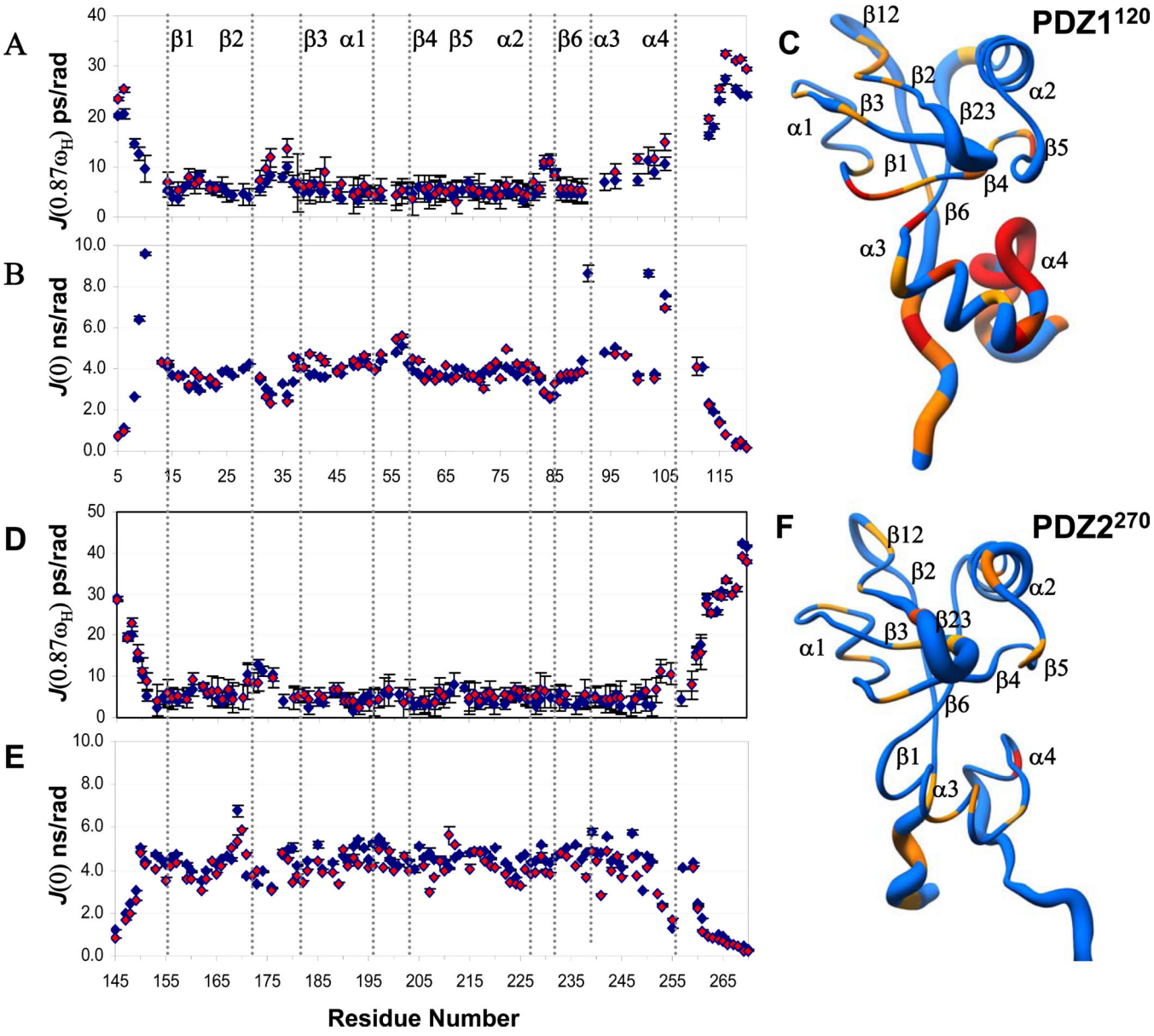

Figure 7. Ligand induced dynamic changes in PDZ1 and PDZ2 domains

Backbone profile of the spectral density function calculated from relaxation measurements at 500 MHz, for PDZ1^{120} in the presence (red) and absence (blue) of CFTR-C peptide. **(A)** $J(0.87\omega_H)$ and **(B)** $J(0)$. (**C**) The radius-of-worm representation of the backbone of PDZ1^{120} in the absence of ligand is scaled by the amplitude of the $J(0.87\omega_H)$ values. The fast timescale picosecond motions are reflected by a thicker tube with residues undergoing slow conformational exchange painted yellow. The presence of slower motions were detected from the ratio of $J(0)^{900}/J(0)^{500} > 1.2$. Resonances broadened beyond detection are colored in red. In the panels (**D**)-(**F**) the corresponding graphs for PDZ2^{270} are displayed.

J Mol Biol. Author manuscript; available in PMC 2014 July 24.

Table 1

CFTR-C Binding Affinity for PDZ Domains from NHERF1.

PDZ Domain	CFTR-C peptide (1475-1480)[#]	CFTR-C domain (1411-1480)[*]	$\Delta G_{N->D}$ kcal/mol	$\Delta H_{N->D}$ kcal/mol	Tm (°C)
PDZ1 (11-99)		298 ± 10 nM	2.6	33.0	50.0
PDZ1 (11-120)	365 ± 35 nM	211±9 nM	6.6	52.9	56.0
PDZ1 (H27N)		312±15 nM			
PDZ1 (E43D)		1550±72 nM			
PDZ1(H27N/E43D)		1100±51 nM			
PDZ2 (150-240)		4800 ± 300 nM	-0.3	27.7	22.0
PDZ2 (150-270)	1079 ± 79 nM	267 ± 11 nM	6.7	79.4	52.0

The enthalpy change ($\Delta H_{N->D}$) and midpoint of thermal unfolding (**Tm**) were obtained from CD melt curves, with corresponding $\Delta G_{N->D}$ of unfolding calculated at 15°C for PDZ1 and 25°C for PDZ2 domains.

[*] Binding affinities of *wild type* and mutant PDZ1 for CFTR-C domain measured by SPR at 15°C and those of PDZ2 domain at 25°C (Li et al, 2005).

[#] Previously published values (Cushing *et al*, 2008) measured from N-terminal tagged peptides by fluorescence at 24°C.

Table 2

Statistics for NMR Ensemble of 20 Structures.

Constraints	**apo PDZ1^{120}**	**PDZ1^{120}+peptide**	**PDZ2^{270} + peptide**
Intraresidue	610	495 (12)[#]	548 (35)[#]
Sequential	590	461 (1)	562 (5)
Medium-Range	362	226	259
Long-Range	714	452	532
Intermolecular		25	27
Total	2276	1672	1968
Dihedral	112	118	122
PDB	2m0t	2m0u	2m0v
BMRB	18824	18825	18826
Precision[*] (Å)			
Structured Regions	0.52 ± 0.11 (1.03 ± 0.11)	0.52 ± 0.07 (1.08 ± 0.09)	0.48 ± 0.10 (0.89 ± 0.09)
Full Chain	0.64 ± 0.10 (1.14 ± 0.10)	0.63 ± 0.08 (1.20 ± 0.09)	0.68 ± 0.10 (1.11 ± 0.09)
Full Chain + peptide		0.63 ± 0.07 (1.20 ± 0.09)	0.67 ± 0.10 (1.12 ± 0.09)
Ramachandran[*]			
Favored regions	87.4%	85.8%	90.4%
Additional allowed regions	10.9%	12.8%	9.3%
Generously allowed regions	1.2%	0.6%	0.1%
Disallowed regions	0.5%	0.8%	0.2%
Energies	(CNS/ARIA)		
<Distance> (Å) d > 0.5Å	0.0	0.0	0.0
<Distance> (Å) d > 0.3Å	0.3	0.1	0.3
<Angle> θ > 5°	0.0	0.0	0.2
E_{Total} (kcal mol^{-1})	-4492 ± 102	-4808 ± 121	-5199 ± 103
E(noe)	40 ± 1	29 ± 3	34 ± 2
E(vdw)	-1001 ± 51	-1045 ± 17	-1122 ± 13

In PDZ2^{270} the structured regions include: β1(153-158), β2(166-169), β3(178-182), β4(198-202), β5(205-206), β6(225-231), α1(187-191), α2(212-220), α3(233-241), α4(248-252), full chain (153-252) and peptide (3-5) were used in the RMSD calculations.

[#]The bracketed numbers represent the peptide restraints.

[*]The backbone (heavy atom) RMSD and Ramachandran plot were calculated for regular secondary structure elements. In PDZ1^{120} the structured regions include: β1(13-18), β2(26-30), β3(37-42), β4(58-62), β5(65-66), β6(85-91), α1(47-51), α2(72-79), α3(93-100), α4(109-112), full chain (13-112) and peptide (3-5) were used in the RMSD calculations.

Table 3

Analysis of Hydrogen Bond Statistics

H-bond/Salt Bridge		**X-ray***	**PDZ1^{120} + pept#**		**PDZ2^{270} + pept#**
Peptide	**PDZ1^{120}**	**Å**	**d < 3.5 Å**	**PDZ2^{270}**	**d < 3.5 Å**
Leu^{0} O	**24 Tyr N**	2.68	2.62-3.47 (60%)	**164 Tyr N**	2.65-3.46 (100%)
Leu^{0} OXT	**24 Tyr N**	3.36	2.58-3.11 (90%)	**164 Tyr N**	2.73-3.22 (100%)
Leu^{0} OXT	**25 Gly N**	2.81	2.53-2.77 (75%)	**165 Gly N**	2.61-3.46 (90%)
Leu^{0} O	26 Phe N			166 Phe N	2.77-3.21 (60%)
Leu^{0} OXT	26 Phe N	3.24	2.85-3.50 (25%)	166 Phe N	2.81-3.13 (40%)
Leu^{0} N	**26 Phe O**	2.78	2.60-2.88 (100%)	**166 Phe O**	2.66-2.95 (100%)
Arg^{-1} N				167 Asn OD1	3.26-3.41 (25%)
Arg^{-1} NH1	22 Asn O	2.96		162 Ser O	
Arg^{-1} NH2	22 Asn O	2.49	2.67-3.08 (20%)	162 Ser O	
Arg^{-1} NE	43 Glu OE2	2.87		183 Asp OD2	
Arg^{-1} NH2	43 Glu OE2	2.94	2.64-3.29 (20%)	183 Asp OD2	
Thr^{-2} O				**167 Asn ND2**	2.74-3.44 (70%)
Thr^{-2} O	**28 Leu N**	2.85	2.71-2.99 (90%)	**168 Leu N**	2.64-2.87 (100%)
Thr^{-2} OG1	**72 His NE2**	2.74	2.64-2.80 (75%)	**212 His NE2**	2.60-2.79 (100%)
Asp^{-3} OD1	27 His ND1	2.55	2.58-2.94 (25%)	167 Asn ND2	
Asp^{-3} OD2	27 His ND1	3.56	2.54-3.44 (40%)	167 Asn ND2	
Asp^{-3} OD2	40 Arg NH1	2.93		180 Arg NH1	
Asp^{-3} OD1	40 Arg NE		2.59-3.40 (25%)	180 Arg NE	
Asp^{-3} OD1	40 Arg NH1		2.65-3.43 (20%)	180 Arg NH1	

Critical intermolecular contacts involving the Type 1 PDZ motif are highlighted in grey.

*The intermolecular hydrogen bonds listed are taken from the published X-ray structure (PDB 1I92) of the canonical PDZ1 domain complexed with CFTR peptide (EQDTRL).

#Using standard definitions, the heavy atom distance between potential H-bond donors and acceptors (<3.5 Å) was calculated from the ensemble of twenty NMR structures. For each complex, pair-wise H-bond interactions satisfied by at least 20% of the structures reported along with the range of distances generated by MOLMOL.